Ergonomic Exoskeleton Synthesis

Application to a Wearable Passive Exoskeleton for the Shoulder

N. van Dijk

TU Delft

Ergonomic Exoskeleton Synthesis

Application to a Wearable Passive Exoskeleton for the Shoulder

by

N. van Dijk

To obtain the degree of Master of Science
At the Delft University of Technology,
To be defended publicly on Friday June 1, 2017 at 12:00 PM.

Student number:	4168143	
Project duration:	September 11, 2017 – June 1, 2018	
Thesis committee:	dr. ir. D. H. Plettenburg,	TU Delft, supervisor
	Prof. dr. ir. J. L. Herder,	TU Delft, supervisor
	Ir. W. W. P. J. van de Sande,	TU Delft, coach

Cover image obtained from [1]

TU Delft

Preface

This thesis concludes my time at the Delft University of Technology for now. I started my time in Delft at the aerospace engineering faculty but after my bachelors I discoverd that I am most interested in the interaction between human and machine. I continued my journey at the Biomechanical design department in Delft. This interest in the human-machine interaction is also the basis of this thesis.

The thesis was performed at Laevo, a small company in Yes!Delft but with great people. This thesis would not be lying here in front of you without them. I want to thank everyone at Laevo for their time and patience in this project. I enjoyed working together; my questions and problems were always handled with great care. The weekly meeting with other students provided a good way of receiving feedback on my work.

I especially want to thank Bas Wagemaker for being my helping hand in manufacturing the prototype and for contributing to the force-deflection behaviour analysis. Although we worked together in the most stressful period of my thesis I did enjoy working with you (although it might have not always appeared that way).

I want to thank Werner van de Sande for being my coach and listening to the challenges I was facing every two weeks. Your criticism was always useful and lifted me to a higher level. It forced me to broaden my vision and look beyond the ordinary.

Finally I want to thank Dick Plettenburg and Just Herder for being my supervisors and for always finding a time to meet all together. This was not always easy to arrange but we succeeded every time. Your criticism was always on point and opened up new perspectives.

N. van Dijk
Delft, May 2018

Contents

1 Introduction

We all want to start and end our day happily and healthy, unfortunately for many this is not the case. Due to physically demanding jobs people suffer from musculoskeletal disorders (MSDs), which are conditions that concern nerves, tendons, muscles and other supporting structures of the body [30]. The result is that people are struck with discomfort and pain in their daily lives.

Even though many labour activities have been taken over by machines nowadays, little decrease in these MSDs has been reported [26] and thus this problem still persists; around 44 millions EU workers are affected annually by MSDs associated with a cost of 240 billion [4]. It has been shown that factors as awkward posture [18, 21, 25, 27, 29, 34, 35, 37, 39], static loading [12, 14, 21], excessive force [21, 28, 29, 35, 37] and repetitive motion [21, 28, 29, 35, 37] are a risk factor in developing MSDs. The sectors that are most exposed to these risk factors are: construction, logistics and manufacturing [25, 32, 38]. Working activities in these sectors are diverse and flexibility is important [22]. Several solutions have already been implemented in past years [36]. Examples of solutions are: adjustments of the workplace ergonomics, breaks in physical activity or physical therapy. These solutions are often permanent and do not provide the required flexibility or they decrease the time on the work floor.

An emerging field that aims to decrease loads in the human body is the field of exoskeletons [13]. In this field the human-machine interaction is more important than ever since a physical interface between human and machine is present. Bad ergonomic design can not only lead to discomfort but can also cause harm to the user and can hereby increase the risk on MSDs even more. Current technology focuses on mechanical design and efficiency rather than on the human-machine interaction [9]. Ergonomics usually comes later in the design process and a more proactive design approach towards ergonomics should be taken [19].

Methods of designing more ergonomic exoskeletons have been proposed [5, 33] and applied [6, 17]. However these applications lack a systematic way of creating the right configurations. This thesis proposes a method that can be used as a tool to systematically design exoskeletons based on ergonomic metrics, this is done by a kinematic synthesis and optimization. The approach extends existing methods that focus on self aligning mechanisms. This extension is done by using the prescribed theory to create self aligning mechanisms and synthesizing all possible configurations with this theory. This set can then be narrowed down. The length of the links for the configurations in this reduced set can then be synthesized. Within this set an optimization is performed to make a trade off between several objectives that are based on ergonomic guidelines. This way all options are take into account and are systematically reduced. Giving the designer a good basis for design choices.

Not only kinematics play a role in ergonomics. The kinetic part is important as well. Shear forces and high pressures on the skin can cause injuries [42]. The proposed method is extended upon by a force-deflection behaviour analysis. The vision of this part is to create a self aligning compliant mechanism since compliant mechanisms have numerous of advantages over conventional mechanisms [15]. The addition of self aligning capabilities would add to these advantages. A step by step plan is presented to come closer to this vision.

The thesis is structured as follows: First a review of the state-of-the-art is done. The technical specifications of the state-of-the-art is presented and the effectiveness and ergonomic performance is investigated. This is followed by the systematic design approach which extends current methods. This systematic design approach is further extended upon by making the step towards a compliant mechanism. An appendix is included which shows the details of the application of the proposed method.

2

Paper: Wearable Passive Upper Extremity Exoskeletons for the Shoulder: A Review

Wearable Passive Upper Extremity Exoskeletons for the Shoulder: A Review

Nick van Dijk

Abstract—Musculoskeletal disorders cause a large amount of the annual sick leaves in the industrial sector. Methods are present to prevent musculoskeletal disorders however these do not provide a solution to all risk factors. Exoskeletons provide a way of reducing loads on the body and hereby decreasing the risks on musculoskeletal disorders. The state-of-the-art of wearable passive upper extremity exoskeletons for the shoulder was investigated categorized and characterized. To identify the state-of-the-art Scopus, Google and Espacenet were used. It was found that there are four different categories in which these devices can be divided: Anthropomorphic/non-anthropomorphic, rigid/soft, only supports upper arm/supports both arms and load adjustable/non load adjustable. The devices were compared on their method of energy storage, weight, distance from the exoskeleton to the body and their support range. Their effectiveness in reducing risk factors was investigated as well as the perceived comfort whilst wearing the device and the interaction forces on the human machine interface of the devices. No strong correlations were found. Compliant structures seem to be the lightest option for storing energy and the load adjustable devices were found to be significantly heavier than the non-load adjustable devices. There seems to be a weak indication that weight is increases with the distance from the body. No correlations were found between the range of support and the distance to the body. Also no correlations were found between the range of support and the weight. There is an indication that gas spring or helical spring devices need a greater distance to the body. Only one device was evaluated in two effectiveness studies, which showed positive results. No research was conducted on perceived comfort whilst wearing the device. Also no research was conducted on the interaction forces on the human-machine interface. More human factors research has to be conducted to draw conclusions and provide guidelines on how to add comfort and increase effectiveness of Wearable passive upper extremity exoskeletons for the shoulder.

Index Terms—Wearable, Exoskeletons, Upper Extremity, Musculoskeletal Disorders, Passive

1 INTRODUCTION

MUSCULOSKELETAL disorders (MSDs) are a major cause of sick leaves in the industry, around 44 millions EU workers are affected annually by MSDs associated with a cost of 240 billion [1]. MSDs have been prevalent for a long time and the exposure to risk factors has decreased little over time [2]. It has been shown that factors as awkward posture [3], [4], [5] [6], [7], [8], [9], [10], [11], static loading [10], [12], [13], excessive force [7], [8], [10], [11], [14] and repetitive motion [7], [8], [10], [11], [14] are a risk factor in developing MSDs. The sectors that are most exposed to these risk factors are: construction, logistics and manufacturing [6], [15], [16]. Working activities in these sectors are diverse and flexibility is important [17]. Several solutions have already been implemented in past years [18]. Examples of solutions are: adjustments of the workplace ergonomics, breaks in physical activity or physical therapy. However few solutions are proposed that offer a reduction in load in the human body and provide the flexibility needed in the aforementioned sectors.

An emerging field that aims to decrease loads in the human body is the field of exoskeletons [19]. Some devices rely on active principles, meaning they need an external power source to provide support and others rely on passive principles in which no external energy source is needed. Furthermore most devices focus on specific parts of the body for example: the lower limbs [20], the lower back [21] and the shoulder [22]. The most common locations for MSDs are the lower back, the neck and the shoulders [2], [23]. These sources also show that the lower back is the most prevalent location for MSDs as a result quite some applications aim to reduce the load on the lower back [21], [24], [25] and many of them have been compared by de Looze [26]. Hence this study focuses on wearable passive upper extremity exoskeletons that aim on reducing the load on the shoulder. The goal of this paper is to identify, categorize and characterize the state-of-the art of wearable passive upper extremity exoskeletons for the shoulders.

The search method, how the devices are categorized and how they are characterized are presented in this paper as well as the search results and the obtained data. This is followed by a discussion on the results. Finally the concluding remarks are given.

2 METHODS

This study provides an investigation of the state-of-the-art of wearable passive upper extremity

exoskeletons for the shoulder. The goal of these exoskeletons is to relieve load on the shoulders. This is often achieved by providing a supportive force that equals the force on the shoulder. This force is a result of both the weight of the arms and external forces present on the arms. If this supportive mechanism, also called a balancing mechanism, does not need external energy sources to provide the supportive force it is referred to as passive.

Devices are considered wearable if they are only connected to the human and not to other external attachment points in any way.

The search scope is defined as wearable exoskeletons that (partially) relieve the shoulder joint from forces acting on it and in which the balancing mechanism is passive.

For the identification of the state-of-the-art three search engines were used: Scopus [27], Espacenet [28] and Google [29]. The search scope mentioned earlier is best described by the keywords shown in table 1. Each column is separated with an AND operator between keywords and in each row every term is separated with an OR operator (i.e. the first column would be Exo* OR ”Wearable Pre/2 device” OR Orthosis). The first column includes different kinds of wearable devices, the second column includes papers that concern parts of the upper extremity, the third column includes results with certain functionalities, the fourth includes different applications of these devices and the last excludes unfavourable terms. These exclusive terms were only searched for in the title. Furthermore the same set of keywords was used in Google to find commercially available devices of which no scientific paper or patent could be found. After completing the search cross referencing was done to find other relevant articles. The articles were judged on their titles, figures and tables and if found relevant enough the abstract was read. After reading the abstract some papers were excluded before proceeding to a more detailed analysis since they were out of the defined scope (i.e. they included active systems, non-mobile systems or systems just for the elbow).

TABLE 1
Overview of search queries used in the Scopus and Espacenet search engines

AND	Exo*
	”Wearable Pre/2 device”
	Orthosis
AND	”Upper Limb”
	”Upper Extremity”
	”Upper Body”
	Shoulder
	Arm
AND	Augment*
	Enhance
	”Gravity Compensation”
	Support
	Assistive
	Balanc*
AND	Passive
	Compliant
	Industrial
	”Body Powered”
	Surgeon
	Industry
	”Manual Labour”
	”Overhead Work”
	”Automotive”
	Surgery
AND NOT	Wrist
	Active
	Robot*
	Hand
	”Lower Body”
	Hip
	Gait
	Spine

An analysis is performed on the outcome of the search. The found devices are first categorized on the following four criteria.

Is the device anthropomorphic or not, where a device is considered to be anthropomorphic if it mimics the kinematics of the human joints.

Does the device have a rigid or a soft structure. rigid devices are devices in which parts are connected by rigid links, this refers to how different segments are connected not to the connection with the body.

Is the support only provided to the upper arm or both forearm and upper arm.

Is the device load adjustable or not load adjustable, in which load adjustable refers to the device being adjustable during use and when load is applied (i.e. it does not include adjustments to the supportive force by inter changing parts of the system).

After categorization the technical properties of the found exoskeletons are quantified and classified, to do this four different metrics are used.

The first metric is the energy storage method. The main purpose of passive upper extremity exoskeletons is to store the potential energy when lowering the arms and give it back when raising them. For each of the found devices it is determined in what way potential energy is stored.

The second metric is weight, this is an important factor since the device is wearable and a big weight

can increase the loads on the human body. The total mass of each device is determined, however not all found sources included the weight of the device and for some an estimate is made based on used material and structural dimensions.

The third metric is the distance of the structural element furthest away from the body to the body itself. This is a rough estimation of how much volume these devices need in order to operate.

The fourth and final metric is the supported range of the device. This gives an insight in the workspace provided by the devices. The support range is expressed in the angle from which the support starts until the angle at which the support is no longer active. where $0°$ is the position when the hands are down at the side of the body and $90°$ is the position where the arms are stretched out straight in front of the body. In some cases the device provided assistance in adduction/abduction direction, in these cases it is explicitly stated. The found numbers are analysed and compared to see if any correlations are present.

After specifying the technical properties shown above, the effectiveness of the found exoskeletons is shown in terms of reduction in the risk factors: awkward posture, static loading, excessive force and repetitive motion.

Furthermore subjective and objective measures on the ergonomics of the human-machine interface are investigated. These include perceived comfort while wearing the device and interaction forces on the human-machine interface. 1

3 Results

This search resulted in 133 hits on Scopus. Scopus uses different search queries than Espacenet does. The Espacenet search was therefore executed in a less structured manner.

After selection based on the title and figures 41 papers remained. Upon further investigation of the abstract another 32 papers were excluded based on being partly actuated or non-wearable devices or they were review papers. This left 11 papers. A clear overview of the devices and the categories they belong in is presented in figure 1.

Out of the 11 devices eight were found to have an anthropomorphic structure [22], [30], [31], [32], [33], [34], [35], [36]. Most devices had a structure that goes over and around the shoulder [22], [30], [31], [32], [33], [34], [35], [36]. [37], [38] provided support from the hips to the forearm by a structure underneath the arms and [39] has a tower on the shoulder from which a spring like cord is supporting a cuff around the forearm. Furthermore one of the exoskeletons had a soft structure [35].

Six of the found devices provided assistance to the upper arm only [22], [30], [31], [33], [34], [35] the 5 others provide balancing to both fore and upper arm [32], [36], [37], [38], [39]. When providing support to both arms there is a coupling issue between the upper arm and the forearm, the moment on the shoulders depends both on upper and forearm angle. This is usually accounted for by parallelograms [36] however [32] solved this dependency by a novel spring stiffness matrix approach proposed by [40].

Two of the devices are load adjustable [37], [38]. Both load adjustable mechanisms use parallelograms with an iso-elastic spring that runs diagonally through the parallelogram. the ratio between gravity force and spring length remains constant and adjusting the height of the spring creates a change in balancing force.

Now that the devices are categorized they can be further analysed. Table 2 shows an overview of the technical properties of the found exoskeletons.

For the device presented by [31] there was not enough information present to determine the method of energy storage. Three devices have the energy storage mechanism located in cartridge next to the arm [22], [31], [33], two devices have parallelograms linked in series [37], [38], one had the mechanism located at the back [30], four devices have the energy storage mechanism integrated in the structure of the exoskeleton [32], [34], [35], [36] and one of the devices had a system that suspended the arm from a tower located on the shoulder [39]. For the right force profile a cam mechanism is used in some cases [30], [41], [42]. In other systems the spring stiffness and location were carefully selected [32], [34], [36] and some rely on triangular relations [37], [38].

The found energy storage methods were combined into four groups: leaf springs, gas springs, helical springs and compliant structures, in which the latter includes soft materials like textiles and rubber and springs that offer stiffness by structural bending with the exception of leaf springs. Figure 2 gives an overview of the weight of the devices in each group of energy storage methods.

The weight of the devices ranges from 0.5 $[kg]$ to 12 $[kg]$. The distance to the body ranges from 10 $[mm]$ to 500 $[mm]$. A clear overview of the support range and all other variables is presented in table 2.

TABLE 2
Overview of state-of-the-art upper extremity passive exoskeletons technical properties

Device	**Energy Storage Method**	**Weight** $[kg]$	**Distance from body** $[mm]$	**Support Range** $[deg]$
Skelex [30] [43]	Leaf Spring	2.5	50	$0-180$
ShoulderX [31]		4.8	80	
Ekso Works Vest [22] [41]	Gas spring	4.3	135	$90-180$
A-Gear [44] [32] [45]	Rubber bands	1.5	50	$70-150$
Levitate [46] [42]	Leaf spring	2.4	70	$90-180$
H. Hsieh (2014) [34]	Flexural spring	0.5	10	$30-120$ (in abduction/adduction)
R. Altenburger (2016) [37]	Helical spring	7.6	500	$45-135$
Y. Zhu (2017) [38]	Gas spring	12	400	$30-150$
SEns [35]	Textile	0.5	20	
Z. Cheng (2015) [36]	Torsional Compliant Beams	0.5	45	$5-175$
Dubey (2011) [39]	Helical spring	0.6	210	$20-70$

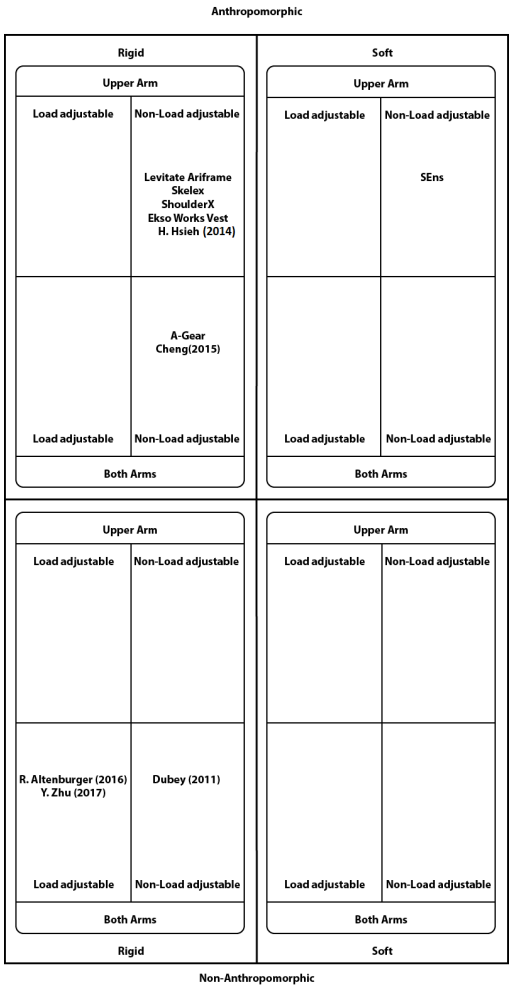

Fig. 1. Overview of the categorization of the state-of-the-art of wearable passive upper extremity exoskeletons for the shoulder

The weight is plotted against the distance from the body in figure 3. It can be seen that there is a slight increase in mass for the devices that have a larger distance from the body ($R^2 = 0.6457$).

The support range per group of energy storage method is plotted in figure 4. Note that the range of support was not known for every found device hence not all 11 devices are presented in figure 4.

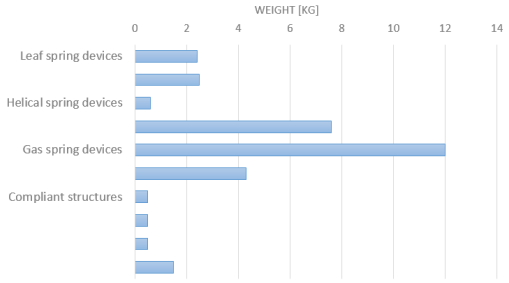

Fig. 2. Weight of devices by energy storage methods divided in the categories leaf springs, gas springs, helical spring and compliant structures

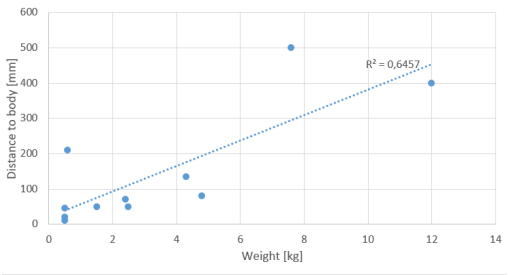

Fig. 3. Weight of all devices plotted against the structural point furthest away from the body with a linear regression fit ($R^2 = 0.6457$)

Figure 5 shows the weight of the devices plotted against their respective support range. The support range is the maximum angle of support minus the minimum angle of support. Again not all 11 devices provided the necessary information needed to include them in the figure.

The relation between the distance to body and the range of motion is shown in figure 6.

Figure 7 shows the distance to body for every device within the defined categories.

These metrics provide an insight in the technical specifications and the correlations between them,

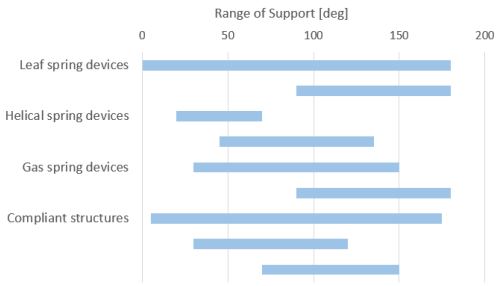

Fig. 4. Range of support with the arms at the side of the body being $0°$ and the arms stretched out straight in front of the body being $90°$, grouped by energy storage methods divided in the categories leaf springs, gas springs, helical spring and compliant structures

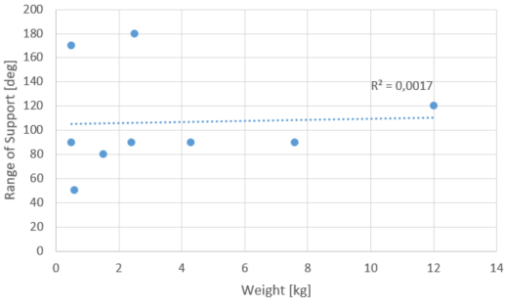

Fig. 5. Weight of devices plotted against their respective range of support, where the range of support is defined as the minimum support angle minus the maximum support angle with a linear regression fit ($R^2 = 0.0017$).

however as already mentioned the goal of these exoskeletons is to decrease the risk on MSDs. An overview of the found effectiveness studies and ergonomic measures is presented below.

Out of 11 exoskeletons only two effectiveness studies were found [46] [47]. Both of these studies were performed with the same exoskeleton: The Levitate. [47] performed a study in which 42 workers

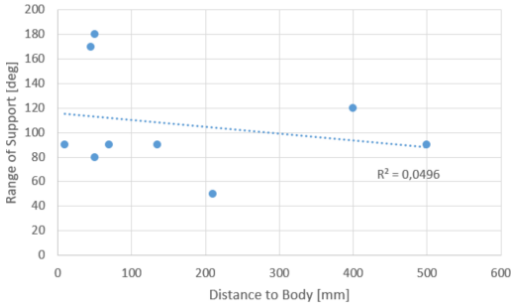

Fig. 6. Distance to body of devices plotted against their respective range of support, where the range of support is defined as the minimum support angle minus the maximum support angle with a linear regression fit ($R^2 = 0.0496$).

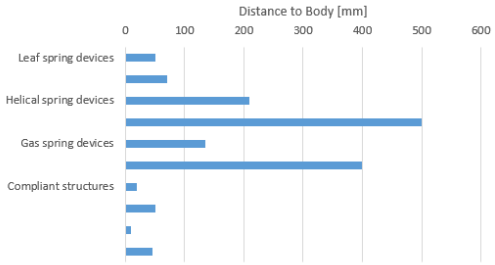

Fig. 7. Distance to body grouped by energy storage methods divided in the categories leaf springs, gas springs, helical spring and compliant structures

from assembly plants were rated on endurance time, posture and precision level during numerous tasks. At the end of each task an interview was held. The study showed longer endurance times, higher precision on tasks and positive reactions from the interview. [46] performed a study on laparoscopic surgery activities and asses 20 subjects on dexterity, arm pain and fatigue. The study concluded that the device significantly reduced experienced fatigue and arm pain whilst having no significant effects on the dexterity.

No studies were found that investigate the perceived comfort while wearing the device or interactive forces between the device and the human (note that pain and fatigue are considered as a subjective measure of risk factor reduction and therefore [46] belongs to the effectiveness studies).

4 Discussion

Since there are not a large number of devices no significant conclusions can be drawn. However indications are presented that give insight in the current state-of-the-art.

When consulting figure 2 it seems like compliant structures are the lightest solutions currently implemented and gas spring the heaviest. Leaf springs lie in the middle. A reason for this is that compliant structures are more organically shaped and can fit the body closer, also the materials used are lightweight and they consist of very few parts. However this comparison does not take into account what functionalities these exoskeletons possess. Helical springs vary a large amount and little can be concluded about them.

Furthermore from table 2 and figure 2 it can be seen that two exoskeletons, the one by Y. Zhu (2017) and R. Altenburger (2016), are significantly heavier than the other devices. From figure 1 it can be seen that both of these devices are load adjustable during use,

hence this functionality imposes a significant amount of additional weight on the system in current devices.

From figure 3 it can also be seen that there is a slight indication that the weight increases with the distance to the body. This can be explained by the amount of material and the larger structures that are required to go around the body. However this weight is also dependent on the choice of material and not directly correlated to the distance to the body.

Figure 4 shows a divided plot with the ranges of support widely spread. Different fields of application apply for different exoskeletons and some manufacturers have chosen for only supporting a specific region, not because of technical limitations, but to maintain a larger freedom of motion.

No correlation can be seen between the range of support and the weight of the device as can be seen in figure 5.

Figure 6 shows no correlation between the range of support and the distance to the body of the device.

From figure 7 it can be seen that helical springs and gas springs show a greater distance to the body then leaf springs or compliant structures. This could be due to the fact that they need a bigger volume to provide the same force. However this can also be caused by design choices or extra functionalities that are added to the system and the location of attachment on the arms. No conclusions can be drawn whether this relation is inherent to the spring type. However, compliant structures do need less parts and can be made very compact [48].

Too little information was found on the effectiveness in decreasing risk factors and no information was found on the ergonomic measures. More human factors research has to be conducted to draw conclusions and provide guidelines on how to add comfort and increase effectiveness of Wearable passive upper extremity exoskeletons for the shoulder.

5 Conclusion

The state-of-the-art of wearable passive upper extremity exoskeletons for the shoulder was investigated, the devices were categorized and their energy storage method, weight, distance from body and the support range was determined. These metrics were compared and an analysis was performed on correlations between these metrics.

No significant results were found during the investigation of the state-of-the-art of wearable passive upper extremity exoskeletons, however there is a slight indication that compliant structures offer the lightest solutions and gas springs the heaviest. Furthermore a larger distance from the body may lead to a higher weight of the device.

The support range with respect to the the energy storage method showed a scattered result and little can be concluded from this. The same can be concluded for the weight with respect to the range of support and the distance to the body with respect to the range of support.

There is an indication that the distance to the body is greater for devices with gas springs or helical springs.

Furthermore it was indicated that adding the possibility to adjust the load may increase the weight of the device drastically.

There is a lack of knowledge present on the effectiveness of wearable passive upper extremity exoskeletons for the shoulder and no research on perceived comfort or interaction forces on the human-machine interface has been conducted.

References

[1] S. Bevan, "The Impact of Back Pain on Sickness Absence in Europe," *The Work Foundation ,Reports*, vol. 1, no. June, pp. 3–8, 2012.

[2] A. Parent-Thirion, G. Vermeylen, G. van Houten, M. Lyly-Yrjänäinen, I. Biletta, J. Cabrita, and I. Niedhammer, *Fifth european working conditions survey*, 2012.

[3] S. F. Wiker, D. B. Chaffin, and G. D. Langolf, "Shoulder posture and localized muscle fatigue and discomfort," *Ergonomics*, vol. 32, no. 2, pp. 211–237, 1989.

[4] U. Järvholm, J. Styf, M. Suurkula, and P. Herberts, "Intramuscular pressure and muscle blood flow in supraspinatus," *European Journal of Applied Physiology and Occupational Physiology*, vol. 58, no. 3, pp. 219–224, 1988.

[5] S. S. Ulin, T. J. Armstrong, S. H. Snook, and W. M. Keyserling, "Perceived exertion and discomfort associated with driving screws at various work locations and at different work frequencies," *Ergonomics*, vol. 36, no. 7, pp. 833–846, 1993.

[6] National Research Council & Institute of Medicine, *MUSCULOSKELETAL DISORDERS AND THE WORKPLACE: Low Back and Upper Extremities*, 2001.

[7] V. Putz-Anderson, B. Bernard, and S. Burt, "Musculoskeletal disorders and workplace factors," *... -Related Musculoskeletal ...*, vol. 97-141, no. July 1997, pp. 1–1 – 7–11, 1997. [Online]. Available: http://scholar.google.com/scholar?hl=en{&}btnG=Search{&}q=intitle:Musculoskeletal+disorders+and+workplace+factors{#}1{%}5Cnhttp://www.cdc.gov/niosh/docs/97-141/pdfs/97-141.pdf

[8] R. M. Van Rijn, B. M. Huisstede, B. W. Koes, and A. Burdorf, "Associations between work-related factors and specific disorders of the shoulder - A systematic review of the literature," *Scandinavian Journal of Work, Environment and Health*, vol. 36, no. 3, pp. 189–201, 2010.

[9] L. Punnett, L. J. Fine, W. Monroe Keyserling, G. D. Herrin, and D. B. Chaffin, "Shoulder disorders and postural stress in automobile assembly work," *Scandinavian Journal of Work, Environment and Health*, vol. 26, no. 4, pp. 283–291, 2000.

[10] B. Larsson, K. Søgaard, and L. Rosendal, "Work related neck-shoulder pain: a review on magnitude, risk factors, biochemical characteristics, clinical picture and preventive interventions," *Best Practice and Research: Clinical Rheumatology*, vol. 21, no. 3, pp. 447–463, 2007.

[11] H. F. van der Molen, C. Foresti, J. G. Daams, M. H. W. Frings-Dresen, and P. P. F. M. Kuijer, "Work-related risk factors for specific shoulder disorders: a systematic review and meta-analysis," *Occupational and Environmental Medicine*, no. i, pp. oemed–2017–104 339, 2017. [Online]. Available: http://oem.bmj.com/lookup/doi/10.1136/oemed-2017-104339

[12] E. Grandjean and W. Hünting, "Ergonomics of posture-Review of various problems of standing and sitting posture," *Applied Ergonomics*, vol. 8, no. 3, pp. 135–140, 1977.

[13] J. A. Hidalgo, A. M. Genaidy, R. Huston, and J. Arantes, "Occupational biomechanics of the neck: a review and recommendations," pp. 165–181, 1992.

[14] L. Punnett and D. H. Wegman, "Work-related musculoskeletal disorders: The epidemiologic evidence and the debate," *Journal of Electromyography and Kinesiology*, vol. 14, no. 1, pp. 13–23, 2004.

[15] D. Wang, F. Dai, and X. Ning, "Risk Assessment of Work-Related Musculoskeletal Disorders in Construction: State-of-the-Art Review," *Journal of Construction Engineering and Management*, vol. 141, no. 6, p. 04015008, 2015. [Online]. Available: http://ascelibrary.org/doi/10.1061/{%}28ASCE{%}29CO.1943-7862.0000979

[16] B. Silverstein and D. Adams, "Work-related Musculoskeletal Disorders of the Neck , Back , and Upper Extremity in Washington State ,," no. 40, pp. 1997–2005, 2007.

[17] M. P. D. Looze, F. Krause, and L. W. O. Sullivan, "Wearable Robotics: Challenges and Trends," vol. 16, pp. 195–199, 2017. [Online]. Available: http://link.springer.com/10.1007/978-3-319-46532-6

[18] D. Van Eerd, C. Munhall, E. Irvin, D. Rempel, S. Brewer, A. J. van der Beek, J. T. Dennerlein, J. Tullar, K. Skivington, C. Pinion, and B. Amick, "Effectiveness of workplace interventions in the prevention of upper extremity musculoskeletal disorders and symptoms: an update of the evidence," *Occupational and Environmental Medicine*, vol. 73, no. 1, pp. 62–70, 2016. [Online]. Available: http://oem.bmj.com/lookup/doi/10.1136/oemed-2015-102992

[19] E. Guizzo and H. Goldstein, "The rise of the body bots," *IEEE Spectrum*, vol. 42, no. 10, pp. 50–56, 2005.

[20] "Lockheed Martin Fortis." [Online]. Available: https://www.lockheedmartin.com/us/products/exoskeleton.html

[21] "Laevo." [Online]. Available: http://www.laevo.nl/

[22] "Ekso Works Vest Sell Sheet," 2015. [Online]. Available: http://2t2ine2n47g337am722tf6ek.wpengine.netdna-cdn.com/wp-content/uploads/2017/07/EksoVest-Sell-Sheet.pdf

[23] P. W. Buckle and J. Jason Devereux, "The nature of work-related neck and upper limb musculoskeletal disorders," *Applied Ergonomics*, vol. 33, no. 3, pp. 207–217, 2002.

[24] "Back X by Suit X." [Online]. Available: http://www.suitx.com/backx

[25] "No Title." [Online]. Available: https://www.cyberdyne.jp/english/products/Lumbar{_}CareSupport.html

[26] M. P. de Looze, T. Bosch, F. Krause, K. S. Stadler, and L. W. O'Sullivan, "Exoskeletons for industrial application and their potential effects on physical work load," *Ergonomics*, vol. 59, no. 5, pp. 671–681, 2016. [Online]. Available: http://dx.doi.org/10.1080/00140139.2015.1081988

[27] "Scopus." [Online]. Available: www.scopus.com

[28] "Espacenet." [Online]. Available: https://worldwide.espacenet.com/

[29] "No Title." [Online]. Available: www.google.com

[30] "Skel-Ex — Home." [Online]. Available: http://skel-ex.com/

[31] "shoulderX — suitX." [Online]. Available: http://www.suitx.com/shoulderx

[32] M. P. Lustig, "A statically balanced mobile arm support based on a novel spring system," 2015. [Online]. Available: http://repository.tudelft.nl/islandora/object/uuid{%}3A200150c2-f399-4353-be34-d42113e0228e?collection=education{%}5Cnhttp://repository.tudelft.nl/islandora/object/uuid{%}3A200150c2-f399-4353-be34-d42113e0228e/datastream/OBJ/view

[33] "Levitate Brochure." [Online]. Available: http://www.levitatetech.com/Levitate-brochure.pdf

[34] H.-C. Hsieh and C.-C. Lan, "A lightweight gravity-balanced exoskeleton for home rehabilitation of upper limbs," *2014 IEEE International Conference on Automation Science and Engineering (CASE)*, pp. 972–977, 2014. [Online]. Available: http://ieeexplore.ieee.org/lpdocs/epic03/wrapper.htm?arnumber=6899444

[35] Y. Kurita, J. Sato, T. Tanaka, M. Shinohara, and T. Tsuji, "Unpowered Sensorimotor-Enhancing Suit Reduces Muscle Activation and Improves Force Perception," *IEEE Transactions on Human-Machine Systems*, pp. 1–6, 2017.

[36] Z. Cheng, S. Foong, D. Sun, and U. X. Tan, "Towards a multi-DOF passive balancing mechanism for upper limbs," *IEEE International Conference on Rehabilitation Robotics*, vol. 2015-Septe, pp. 508–513, 2015.

[37] R. Altenburger, D. Scherly, and K. S. Stadler, "Design of a passive, iso-elastic upper limb exoskeleton for gravity compensation," *ROBOMECH Journal*, vol. 3, no. 1, p. 12, 2016. [Online]. Available: http://robomechjournal.springeropen.com/articles/10.1186/s40648-016-0051-5

[38] Y. Zhu, G. Zhang, H. Li, and J. Zhao, "Automatic load-adapting passive upper limb exoskeleton," *Advances in Mechanical Engineering*, vol. 9, no. 9, p. 168781401772994, 2017. [Online]. Available: http://journals.sagepub.com/doi/10.1177/1687814017729949

[39] V. N. Dubey and S. K. Agrawal, "Study of an upper arm exoskeleton for gravity balancing and minimization of transmitted forces," *Proceedings of the Institution of Mechanical Engineers, Part H: Journal of Engineering in Medicine*, vol. 225, no. 11, pp. 1025–1035, 2011. [Online]. Available: http://journals.sagepub.com/doi/10.1177/0954411911420664

[40] P.-Y. Lin, W.-B. Shieh, and D.-Z. Chen, "A stiffness matrix approach for the design of statically balanced planar articulated manipulators," *Mechanism and Machine Theory*, vol. 45, no. 12, pp. 1877–1891, 2010. [Online]. Available: http://linkinghub.elsevier.com/retrieve/pii/S0094114X10001370

[41] E. Bionics, "Exoskeleton and method of providing an assistive toruque to an arm of a wearer," 2017.

[42] L. T. Inc., "Exoskeleton and method of providing an assistive toruqeu to an arm of a wearer," 2016.

[43] I. de Looij, "Modeling and altering the force profile of a spring-based upper body exoskeleton with design adjustments," 2017.

[44] A. G. Dunning, *Slender spring systems*, 2016.

[45] P. N. Kooren, A. G. Dunning, M. M. H. P. Janssen, J. Lobo-Prat, B. F. J. M. Koopman, M. I. Paalman, I. J. M. de Groot, and J. L. Herder, "Design and pilot validation of A-gear: a novel wearable dynamic arm support," *Journal of NeuroEngineering and Rehabilitation*, vol. 12, no. 1, p. 83, 2015. [Online]. Available: http://www.jneuroengrehab.com/content/12/1/83

[46] S. Liu, D. Hemming, R. B. Luo, J. Reynolds, J. C. Delong, B. J. Sandler, G. R. Jacobsen, and S. Horgan, "Solving the surgeon ergonomic crisis with surgical exosuit," *Surgical Endoscopy and Other Interventional Techniques*, pp. 1–9, 2017.

[47] L. Gastaldi and M. P. Cavatorta, "Advances in Physical Ergonomics and Human Factors," vol. 602, no. i, 2018. [Online]. Available: http://link.springer.com/10.1007/978-3-319-60825-9

[48] L. L. Howell, "Introduction to Compliant Mechanisms Mechanisms," 2013.

3

Paper: A Systematic Approach to Ergonomic Exoskeleton Design

A Systematic Approach to Ergonomic Exoskeleton Design

Nick van Dijk, Werner W.P.J. van de Sande, Dick H. Plettenburg, Just L. Herder

Abstract—The human machine-interface is more important than ever in the field of exoskeletons. Current design approaches lack a way of systematically designing the ergonomics of exoskeletons. Methods with a more pro active approach to ergonomics have to be developed. This paper extends existing methods by which self aligning mechanisms are created with a systematic approach. A synthesis method is proposed by which all possibilities are synthesized. These possibilities are then excluded based on kinematic requirements on the system. The remaining possibilities are optimized based on ergonomic guidelines to obtain a set of solutions from which the designer can make well founded design choices. This proposed method is applied to a planar passive exoskeleton for the shoulder. The method was successfully applied by using the total link length, reachable workspace, distance to the body and singularity avoidance as objectives for the optimization. the resulting objective values were verified by means of a prototype. The test results showed to be within reasonable bounds to verify the method for the planar case. The proposed method can be used as a tool in future exoskeleton design and can be extended with additional objective functions and constraints and can be extended to the three dimensional case.

Index Terms—Exoskeleton design, kinematic synthesis, optimization, ergonomics

1 INTRODUCTION

Exoskeletons are seen more and more in the daily lives of people [1]. The purpose of these devices can range from augmenting human capabilities to rehabilitation, however they all have one thing in common: A physical interaction between human and machine is required [2]. Design flaws do not only lead to discomfort but harm might be done to the user. Hence in this field the human-machine interaction is more important than ever. However, current technology focuses on mechanical design and efficiency rather than on the human-machine interaction [3]. Ergonomics usually comes later in the design process and a more proactive design approach towards ergonomics should be taken [4]. This is further confirmed by Schiele [5]

Both kinematics and kinetics play a large role in the interaction between human and machine. Kinematic incompatibility and providing inappropriate forces could lead to unwanted interaction forces which may cause harm to the user. One of the main causes of unwanted interaction forces is the misalignment of the human joint with the exoskeleton [5]. Replication of the human limb kinematics has failed too often due to the high variability between subjects and the complex movement patters of the human joints [6]. Schiele and van der Helm [7] made an effort to tackle this problem by creating a self aligning mechanism (SAM) and Stienen et al. [8] proposed to decouple rotations and translations and hereby creating adaptive degrees of freedom by which the exoskeleton can align itself with the human joints axes. Cempini et al. [9] propose a method that describes the general proof and method of designing self aligning exoskeletons. This method has been successfully applied numerous of times [10], [11]. However none of these designs has a systematic way of coming to a final design. Often little justification is given for design choices [12], this leads to configurations that are potentially sub-optimal.

This paper aims to extend existing methods that overcome the misalignment issue with a systematic approach. This systematic approach takes a proactive attitude towards ergonomics and incorporates this into the design process. By taking a systematic design approach the designer makes sure that all design choices are well founded and that he or she avoids missing out on optimal configurations. Incorporating ergonomics into this systematic approach ensures that a baseline of ergonomic performance is present and promotes a proactive attitude towards ergonomics.

The method proposed by Cempini [9] is taken as a basis for self aligning mechanisms and is extended upon. This extension is done by a kinematic synthesis. This synthesis approach makes sure all possibilities are considered in the design process and that no optimal solutions are missed. The mathematical expressions used in Cempini [9] can be used to synthesize all possible self aligning mechanism configurations for a specific case. This set of configurations is then narrowed down by the kinematic requirements of the system. The remaining configurations are further synthesized by determining

all the possible lengths of the connecting elements.

The next step is to select preferred configurations from this set of possibilities, this is done by means of optimization. A more proactive design approach towards ergonomics has to be taken. However quantifying requirements based on ergonomic factors proved to be a challenge in previous exoskeleton design [12]. This quantification is still hard to do and is not an exact science. Often certain ergonomic requirements are in conflict with other functional requirements and a trade-off has to be made. Hard requirements on the system to be designed are therefore difficult to achieve and an optimization algorithm provides a systematic way of performing this trade-off. This optimization takes requirements that are based on ergonomics as an objective.

The outline of the paper is as follows: First the proposed method is discussed, in the chapter thereafter the application to a planar shoulder exoskeleton is presented this is followed by the results of this application. The results are then verified and a discussion follows together with future recommendations. The end of the paper consists of the concluding remarks.

2 Design Methodology

The design methodology in this paper based on the theory presented by Cempini [9]. This theory describes that for a human joint a robotic chain can be connected from the proximal side of the joint to the distal side of the joint. This robotic chain is considered self aligning if the following transformation holds:

$$
\begin{aligned}
&{}^{F}T_{e}^{SAM} = {}^{F}T_{0}(S)\,{}^{0}T_{e}(q) = {}^{F}T_{e}^{Human} \\
&= {}^{F}T_{\tilde{0}}(S,\delta)\,{}^{\tilde{0}}T_{\tilde{0}}(\tilde{q},\delta)\,{}^{\tilde{e}}T_{e}(S)
\end{aligned}
$$

Where ${}^{j}T_{i}$ denotes the transformation matrix from frame j to frame i. The frame definitions are shown in figure 1. In short this equation considers the transformation from a point on the proximal link to a point on the distal link. It shows that the transformation caused by the orientation and location of the SAM is the same as the transformation caused by the orientation and location of the human joint. If this holds the mechanism will be self aligning.

There are two systems that need to work together. The human chain and the self aligning chain. Both systems exist of a number of joints: the joint space. The human chain is modelled by one or more simple rotational joints that cause the movement of limbs as they would in the human body. This is the human joint space. In reality these can not be represented by simple joints since they also slip and slide during motion. For this reason the model also has a number of misalignment joints. These represent the

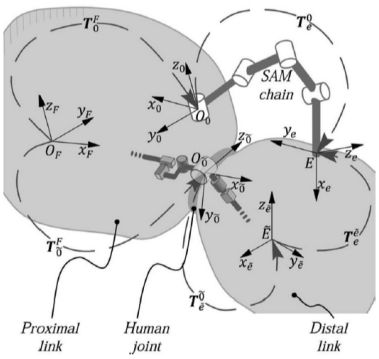

Fig. 1. Human joint with a proximal and a distal link connected with a self aligning mechanism, the transformations are represented by the dotted arrows the figure is adapted from [9]

uncertainty of the rotation centre of the human joints. All of the misalignment joints together are referred to as the misalignment joint space. This human model is referred to as a misalignment model. Some two dimensional examples of these models are shown in figure 2. The human model then consists of a human joint space, defined as $\tilde{q}$ and a misalignment joint space defined as δ. Furthermore Cempini [9] states that the frame orientation and position is described by N variables. In the two-dimensional case $N = 3$ and in the three-dimensional case $N = 6$. The self aligning mechanism that is attached to the human must have at least $n \geq N$ degrees of freedom. The joint space of the self aligning mechanism chain is defined as q. This joint space can be divided into adaptive joints q_a, which are not actuated, and controlling joints q_c, which are actuated. In order for the system not to have redundant joints the amount of adaptive joints has to be less or equal to the misalignment joints:

$$dim(q_a) \leq dim(\delta) \tag{1}$$

For the system to be controllable it has to have at least the amount of controlling joints as there are joints in the human joint space:

$$dim(q_c) \geq dim(\tilde{q}) \tag{2}$$

With this mathematical basis the synthesis can be performed which extends the method proposed by Cempini [9]. The systematic approach that is taken can be summarized in a flow chart and is shown in figure 3. Each station and its corresponding inputs are discussed in this section.

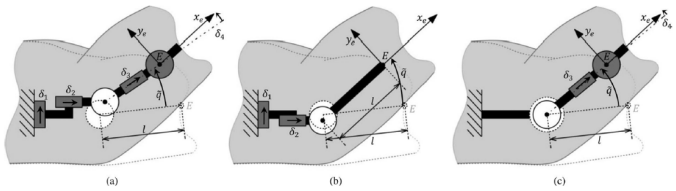

Fig. 2. Misalignment model in which δ presents the misalignment joints and $\tilde{q}$ presents the human joints a) is the case with three misaligning joints b) two misaligning joints and c) has one misalignment joint, the figure was adapted from [9]

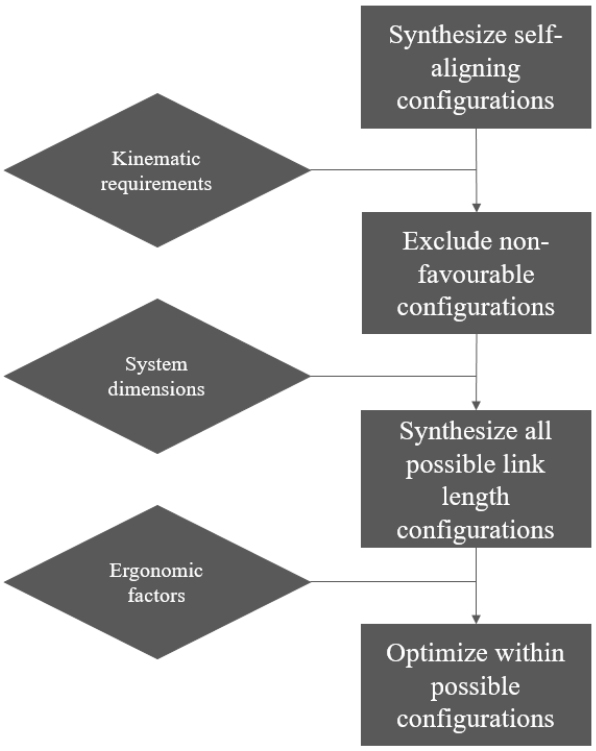

Fig. 3. Proposed design method summarized in a process flow chart, this method is followed throughout this paper

2.1 Synthesize SAM Configurations

In three dimensions six lower kinematic pairs can be considered [13]. All are shown in table 1. The revolute, screw and prismatic pairs have one degree of freedom, the cylindrical pair has two degrees of freedom and both the Spherical and planar have three. The total degrees of freedom of the selected kinematic pairs must equal that of the self aligning mechanism which is equal to n. In two dimensions only two lower kinematic pairs are present, which are also shown in table 1.

2.2 Exclude Configurations

The synthesis of self aligning mechanisms results in a large set of possibilities. A large portion has to be excluded based on the requirements of the entire system until a manageable set of mechanisms is left. The input of these exclusions are based on the kinematic requirements on the system. First of all the human body consists of different joint types. Most of these joints provide rotational movement [14]. This means that the exoskeleton should be able to provide axial movement as well. If this can not be facilitated the exoskeleton is excluded. The exoskeleton should be able to provide the prescribes motion and should not be hindered by singularities. Configurations that are sensitive to singularities are thus excluded. Human dimensions and joint movement impose restrictions on the joints of the exoskeleton. The exoskeleton joints have to stay within a certain region or are limited in their movement. If joint movement exceeds these constraints the configuration is excluded. Furthermore prismatic as well as planar joints could jam if the force has an offset [15]. For this reason configurations with more planar or prismatic joints than other joint types (P-heavy configurations) are excluded. The four reasons that serves as an input for the exclusion of configurations are listed below:

1) Rotational movement can not be facilitated
2) Sensitive to singularities
3) Joint movement exceeds constraints
4) P-heavy

2.3 Synthesize Link Lengths

The self aligning configurations can now be connected with rigid links. The lengths of these links are synthesized. The joint types impose certain geometrical relations on the system. This together with the dimensions of the user(s) and the fact that the links are rigid, and thus can not elongate, dictates the boundaries of these link lengths.

2.4 Optimize

This analysis of link length possibilities results in a large set of possible designs. A trade-off between all of these concepts has to be made, however due to the size of the set this can not be done manually. In order to make this trade-off an optimization algorithm is used. In this algorithm one or more objectives can be defined which are optimized. In the case of one objective this will result in an optimal solution. In the case of multiple objectives it will result in a Pareto front. A Pareto front can be described as a set of solutions. This set of solutions has no other feasible solutions for which one of the objectives values can be increased without decreasing another objective [16]. This Pareto front allows the designer to narrow down the possibilities to only the optimal solutions

TABLE 1
Lower kinematic pairs for creating a self aligning mechanism and their corresponding degrees of freedom

Lower Kinematic Pair	Two Dimensions	Three Dimensions	Degrees of Freedom
Revolute	X	X	1
Prismatic	X	X	1
Screw		X	1
Cylindrical		X	2
Spherical		X	3
Planar		X	3

for him or her.

The physical boundaries of the link lengths is used as a search space for the optimization. The objectives of the optimization are case specific and based on requirements that represent a metric for ergonomic performance, but are hard to turn into an exact requirement. According to a report by the International Ergonomics Association [17] ergonomics can be defined as:"the scientific discipline concerned with the fundamental understanding of interactions among humans and other elements of a system, and the profession that applies theory, principles, data and methods to design in order to optimise human well-being and overall system performance". The International Ergonomics Association prescribes numerous guidelines on different types of ergonomics. The exoskeleton is considered as a tool. Several guidelines exist for tools. The guidelines relevant for the design of the tools are listed below:

1) Body posture needs to be comfortable and stable
2) Handle characteristics should be secure and comfortable
3) balance and weight should make it easy to operate the tool
4) Tool alignment should be easy and give feedback to correct positions

The exact metrics that are used as objectives for the optimization are dependent on the application and the target group. In the application of the method the exact metrics are defined, this is discussed in the next chapter.

3 Application to a Passive Planar Shoulder Exoskeleton

In this paper the proposed design method is applied to a planar passive shoulder exoskeleton meant for assisting healthy subjects in physically demanding tasks. The exoskeleton is attached to the hip and provides support to the upper arm. The exoskeleton should be simple, light and compact. The minimum set of variables in two-dimensional space is three and $dim(q) = n \geq N$. To keep the design as simple as possible the minimum required dimension for the self aligning mechanism is chosen $n = 3$. The human shoulder model used has one rotating degree of freedom and a misalignment joint in the horizontal direction and in the vertical direction. This way the uncertainty of the centre of rotation of the human shoulder can be modelled. This corresponds to the second misalignment model from figure 2. in which $dim(\delta) = 2$ and $\dim(\tilde{q}) = 1$. This results in a self aligning mechanism with $dim(q_c) \geq 1$ and $dim(q_a) \leq 2$. Below the same process is followed as described in the previous section.

3.1 Synthesize SAM Configurations

In the planar case two kinematic pairs can be chosen: The revolute (R) pair and the prismatic pair (P). Furthermore the prismatic pair can be configured in two ways, as shown in figure 4 (a) where blue slides over grey and figure 4 (b) where grey slides over blue. All of the options one degree of freedom to the system and a total of three degrees of freedom need to be present. Hence the whole set of possibilities is described by $3^3 = 27$ configurations.

3.2 Exclude Configurations

The synthesized configurations can now be narrowed down based on the criteria mentioned in the previous section. Table 2 shows on what grounds configurations were excluded according to the reasons mentioned in the previous section. After this analysis three configurations remain: RRR, PRR and RPR. Figre 5 shows the RRR configuration, figure 6 shows the RPR configuration and figure 7 shows the PRR configuration.

3.3 Synthesize Link Lengths

All these configurations have two exoskeleton links and are attached to the arm at some distance to the shoulder. These first two links and the attachment point (AP) to the arm, expressed as a part of the arm length, are the variables used in analysis of all the possible systems and define the bounds and constraints for the optimization problem. All other parameters are taken to be constant.

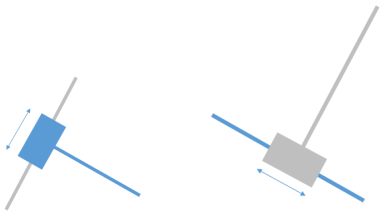

(a) (b)

Fig. 4. Graphical representation of the two prismatic options in which (a) is where blue slides over the grey link and (b) is where grey slides over the blue link

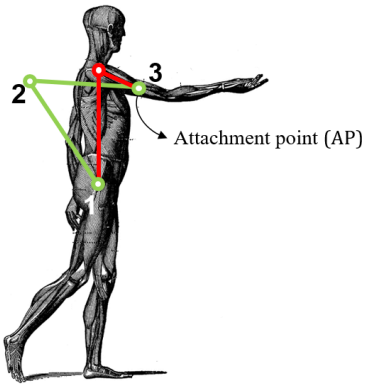

Fig. 5. RRR configuration, three revolute joints in series, the exoskeleton is represented by the green lines and the human skeleton is represented by the red lines

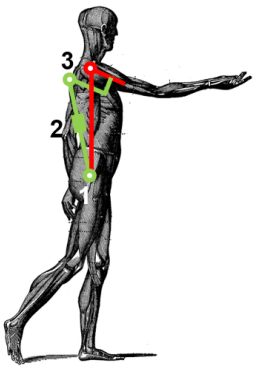

Fig. 6. RPR configuration, a revolute joint followed by a piston type joint in series with another revolute joint, the exoskeleton is represented by the green lines and the human skeleton is represented by the red lines

TABLE 2
Excluded configurations based on the reasons for exclusion in which R stands for a revolute pair and P for a prismatic pair, the subscripts 1 and 2 denotes the first or second option of the prismatic pair

Excluded Trees	Excluded Configurations	Reasons
PPP	$P_1P_2P_2$, $P_2P_1P_2$, $P_2P_2P_1$, $P_1P_1P_2$, $P_1P_2P_1$, $P_2P_1P_1$, $P_2P_2P_2$, $P_1P_1P_1$	1, 3, 4
RPP	RP_1P_2, RP_2P_1, RP_1P_1, RP_2P_2	1, 3, 4
PRP	P_1RP_2, P_2RP_1, P_1RP_1, P_2RP_2	1, 2, 4
PPR	P_1P_2R, P_2P_1R, P_1P_1R, P_2P_2R	4
RRP	RRP_1, RRP_2	1
PRR	P_2RR	1

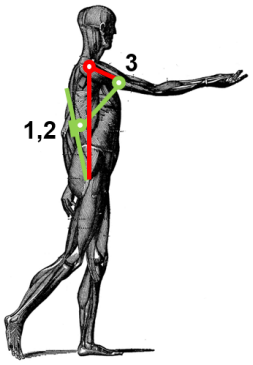

Fig. 7. PRR configuration, a prismatic joint followed two revolute joints, the exoskeleton is represented by the green lines and the human skeleton is represented by the red lines

3.4 Optimize

The focus of the optimization lies on selecting a number of solutions that favour certain ergonomic aspects. In this application four objectives are being optimized. The first objective is based on reducing the weight and decreasing the size of the system. Increased weight will decrease wearing comfort and the size of the system will influence how agile the user is. As mentioned in the previous section: balance and weight should make it easy to operate the tool. Since material types has not been selected the total link length is considered as a good measure for weight. This can mathematically be defined as:

$$f_1(\mathbf{x}) = L_1 + L_2 + AP \cdot L_{arm} \tag{3}$$

in which L_1 is the length of link one, L_2 is the length of link two, AP is the attachment point to the human arm and L_{arm} is the length of the human arm which is taken as a constant. The definitions are more explicitly stated in appendix B.

The second objective aims on preserving the range

of motion of the entire system (i.e. man and machine combined). Decreased range of motion can lead to the user being limited in moving the arms, this can lead to bad body posture, uncomfortable handle characteristics and improper tool alignment. To express the combined range of motion the system is divided into two systems: the exoskeleton and the human arm. The attachment point is where these two systems meet. Then the entire range of motion of the human upper arm is expressed in attachment point coordinates and the same is done for the exoskeleton. Due to the fact that the upper arm can translate as well as rotate this will create an area in Cartesian space in the planar case. The overlap between the two areas is taken and expressed as a percentage of the human workspace area. The inverse of this is minimized which will result in getting as close to $100\ \%$ as possible. The overlapping areas can be expressed as shown in equation 4 and the objective function to be minimized is then showed in equation 5.

$$A_{workspace} = w_{arm} \cap w_{exo} \tag{4}$$

$$f_2(\mathbf{x}) = \frac{w_{arm}}{A_{workspace}} \tag{5}$$

The third objective is to minimize the distance to the human body. Since this application focusses on an industrial environment moving around is essential. If the distance to the body is big the user can bump into objects and body posture as well as handle characteristics could become uncomfortable. To enhance wearing comfort and handle characteristics the exoskeleton should stay close to the body throughout its entire motion in the achievable workspace. For simplicity the body is represented as a line that runs from the hip to the shoulder. The distance of the entire exoskeleton to the body in the three joint configuration is determined by the distance of the second joint to this line. As an objective function the mean of this distance throughout the entire motion is minimized as shown in equation 6.

$$f_3(\mathbf{x}) = \frac{1}{n}\sum_{i}^{n} ||\mathbf{distance}_i||_2 \tag{6}$$

In which subscript i represents the $i-th$ position in the movement throughout the workspace. n is the total amount of points taken throughout the movement through the workspace and depends on the chose accuracy.

The last objective focuses on singularity avoidance. Singularities cause the loss of degrees of freedom of the system and can possibly lead to unwanted interaction forces. This could leed to unstable and uncomfortable body posture and bad handle characteristics. This objective includes singularity avoidance as a penalty barrier for the optimization problem. This is done by determining the jacobian J of the self aligning mechanism at every position i throughout the workspace. Whenever this determinant becomes equal to zero $det(J) = 0$, the system is in a singular configuration. The inverse of this will thus go to infinity. Hence the fourth objective is described by equation 7.

$$f_4(\mathbf{x}) = max(\frac{1}{|det(J_i)|}) \tag{7}$$

In which i denotes the $i-th$ position in the workspace. The maximum value over the entire workspace is taken as an objective to avoid a singular position in the workspace.

The objectives and the objective functions are summarized in table 3 together with their ergonomic motivation based on the four ergonomic guidelines mentioned in the design methodology.

4 Results

First the results of the link length analysis are presented for all three cases followed by the results of the optimization. For this application an exoskeleton that is connected to the hip and supports the upper arm is synthesized. For anthropomorphic data Dined is used [18]. The average vertical distance from hip to shoulder is found to be $0.5\ [m]$. The horizontal is assumed to be $0.1\ [m]$ based on the chest width data from Dined [18]. The length of the upper arm was found to be $0.35\ [m]$ [18]. The attachment point (AP) on the human arm is assumed to be able to run from $20\ \%$ to $80\ \%$ of the upper arm length from the proximal end to keep a safety clearance from the end points of the arm. The required shoulder translation is $5\ [cm]$ in vertical direction [19] and $2\ [cm]$ is horizontal direction [20] . The required angle range of the upper arm with respect to the horizontal line (arms stretched out in front of the subject) is $[-85°, 85°]$.

4.1 Link Length Analysis Results

The link length analysis considers three parameters to be designed for: L_1, L_2 and APs. The result of this analysis is a design volume which sets the boundaries of a physically possible set of link lengths. These physical boundaries are constrained by the fact that a rigid connection from joint to joint has to be made without stretching the link. This should be possible for at least one full stroke from $-85°$ to $85°$ at a shoulder location of $[0.1\ [m],\ 0.5\ [m]]$. This is assumed to be the neutral position. The resulting set of possible link lengths then flows from the joint configurations and the assumed size of the user. The resulting volumes are shown in figure 8 for the RRR case, in figure 9 for the RPR case and in figure 10

TABLE 3
Overview of objective functions, there mathematical expression and the ergonomic factors that are being optimized for corresponding to the four ergonomic guidelines from the design methodology presented in section 2 in this paper

	1.	**2.**	**3.**	**4.**
Objective	Total Link Length	Workspace	Distance To Body	Singularity Avoidance
Objective Function	$L_1 + L_2 + AP \cdot L_{arm}$	$\frac{w_{arm}}{A_{workspace}}$	$\frac{1}{n}\sum_i^n \|\|\mathbf{distance}_i\|\|_2$	$\frac{1}{\|det(J_i)\|}$
Ergonomic motivation	3	1,2,4	1,2	1,2

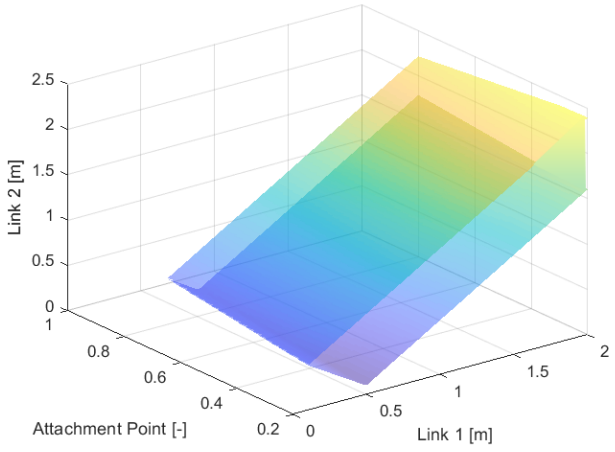

Fig. 8. lower and upper bounds on link two as a function of the attachment point and link one

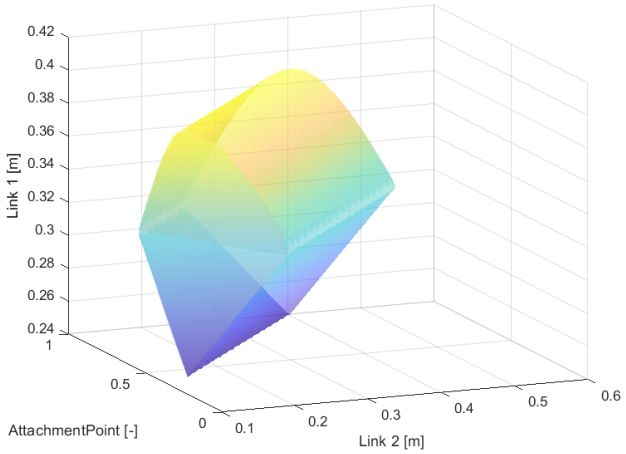

Fig. 9. lower and upper bounds on link one as a function of the attachment point and link two

for the PRR case. Note that for the PRR case the boundary is not a volume but a plane in space. This is due to the fact that link one is determined by the maximum slider range of the first joint. The rail of the slider needs to have the length of the maximum height that this slider needs. This height is unique for every value of link two. All values above this surface are feasible. This would however result in a rail for the slider that is longer than it needs to be.

These boundaries are approximated by a set of linear equations used as constraints for the optimization problem.

4.2 Optimization Problem Definition

The physical boundaries determined in the previous section are used as boundaries for the optimization problem. The problem can thus be formulated in its formal form:

$$\begin{aligned} \min_{\mathbf{x}} \quad & \mathbf{f}(\mathbf{x}) \\ \text{subject to} \quad & A_{eq}\mathbf{x} = b_{eq} \\ & A\mathbf{x} \leq b \\ & h(\mathbf{x}) = 0 \end{aligned}$$

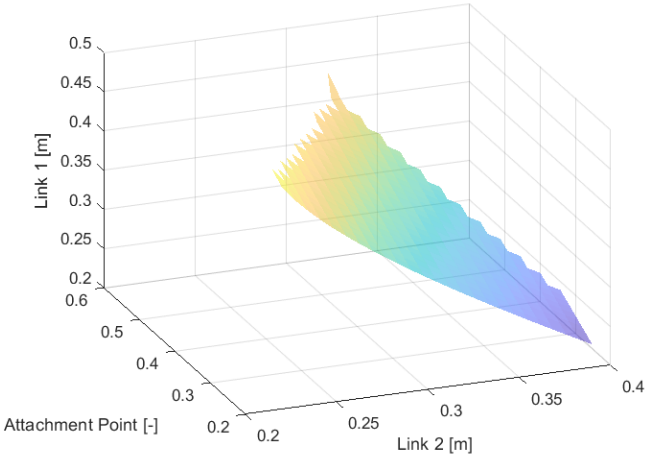

Fig. 10. bounds on link one, link two and the attachment point that have to be satisfied for a feasible PRR linkage

$$g(\mathbf{x}) \leq 0$$

In which $\mathbf{x}$ is the parameter vector, which in this case consists of $[L_1, L_2, AP]$, A_{eq} and b_{eq} are in matrix form and describe the linear equality constraint, A and b are also in matrix form and describe the linear inequality constraints, $h(\mathbf{x})$ describes the non-linear equality constraints and $g(\mathbf{x})$ describes the non-linear inequality constraints. Although boundaries are approximated linearly they do include discontinuities and thus impose a non-linear constraint on the optimization problem. As can be seen in figures 8 9 and 10 the boundaries differ per case. Therefore each case has a different number of linear and non-linear constraints. The linear an non-linear constraints are discussed in more detail in the appendix.

4.3 Optimization Results

The optimization is performed as follows: the algorithm used is the `gamultiobj` algorithm from the `MATLAB` global optimization toolbox. This algorithm can deal with the discontinuities in the constraints and the non-linearities of the objectives as well a do a multi objective optimization. The default parameters were used in the optimization process. The population size is 50 with a crossover fraction of 0.8. The algorithm creates random starting points within the boundary sets. The constraint tolerance is equal to $10e^{-3}$. Since a multi objective optimization is done the result is a Pareto front. The genetic algorithm is initialized with random values, this results in different optimal points in each run. Each run delivers 18 points on the Pareto front. To get a good overview of the Pareto front the optimization is performed five times for each configuration. This results in a total of $18 \cdot 5 = 90$ Pareto optimal solutions.

Although the algorithm incorporates singularity avoidance in the objective function this does not necessarily mean that all singularities are excluded from the solution space. Since singularities are undesired the results that show singular positions are excluded from the solution set. This is done by deleting high values in the outcome of the fourth objective function. Due to rounding errors the determinant of the jacobian is not always exactly 0. A tolerance of $1e^{-3}$ is used meaning that all objective values bigger than $1e^{3}$ are deleted from the solution space.

After deleting these singular values the resulting set for the RRR case counts 77 optimal solutions, the RPR case counts 0 optimal solutions and the PRR case counts 90 optimal solutions. Note that all RPR solutions were found to be singular and hence no further attention is given to these results.

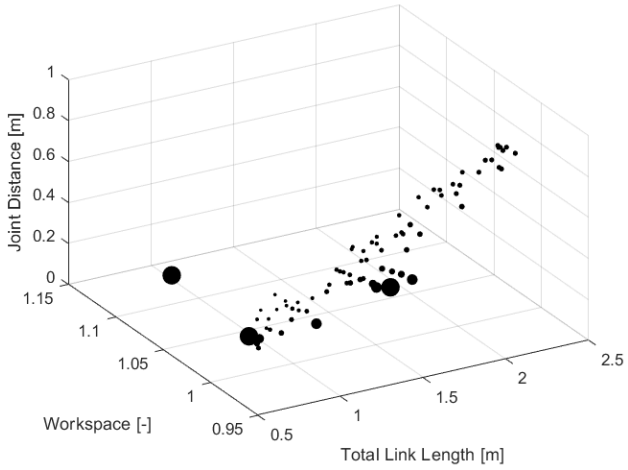

Fig. 11. Pareto front of solution space for the RRR case obtained with the `MATLAB` multi objective genetic algorithm, the bubble size indicates the magnitude of the fourth objective

The result of the multi objective genetic algorithm optimization is a Pareto optimal front. The objective being optimized is four dimensional. This makes visualization a challenge. For this reason a bubble chart is chosen in which the size of the bubbles resembles the inverse of the determinant. The results of the objective values are shown in figure 11 for the RRR case and figure 12 for the PRR case. In figure 11 and 12 it can be seen that the result of the optimization is indeed a Pareto front of solutions. In figure 11 a wider spread is present than in figure 12. Further more the results show values of 0.96 for the second objective (workspace), while the theoretical value can not exceed 1 according to equation 5.

Figure 13 and figure 14 show the possible configurations resulting from the optimization plotted in the earlier defined search spaces. Figure 13 shows that the RRR boundaries on the link lengths are obeyed. In figure 14 it can be seen that the PRR bounds are slightly exceeded. The cause of this is that the approximation of the equality constraint is linear while in reality it is a non-linear boundary. Note that the points all lie above the equality constraint. This region is still physically possible since everything above the surface is an allowable link one length. However the slider only reaches the height that the equality constraint specifies so any added length to link one will be redundant.

5 Validation Method

The used method has to be validated to show the correctness of the method. To do this one configuration of the RRR results and one

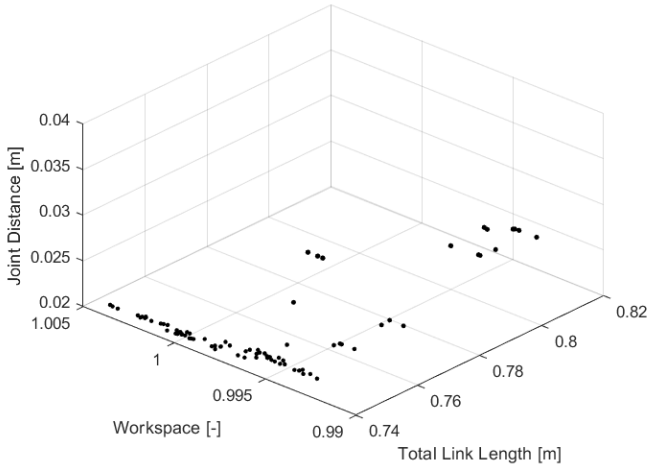

Fig. 12. Pareto front of solution space for the PRR case obtained with the MATLAB multi objective genetic algorithm, the bubble size indicates the magnitude of the fourth objective

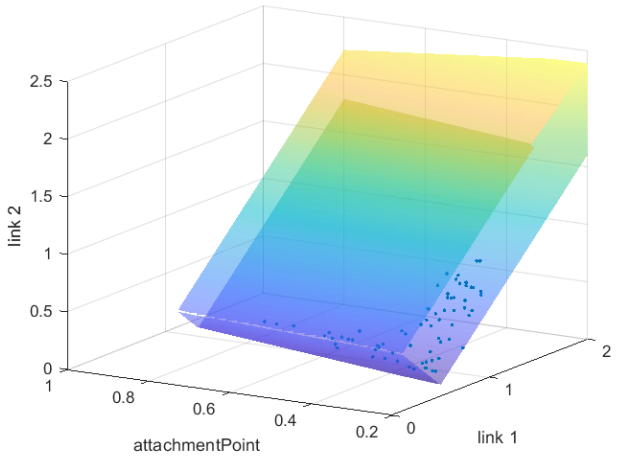

Fig. 13. Scatter plot of the solution space resulting from the optimization for the PRR case plotted in the search space

configuration of the PRR results is chosen to be verified. This choice is based on the configuration being low in sensitivity to uncertainties relative to other solutions in the solution space. The chosen configurations the corresponding link lengths, fitness values and the sensitivity to a $1\ \%$ uncertainty in one of the link lengths are shown in table 4.

These selected configurations are tested on all objective function outcomes. The total link length is trivial to test. This is done by adding all link lengths up. This will result in the total link length and should correspond to the result of the optimization.

To verify the workspace resulting from the

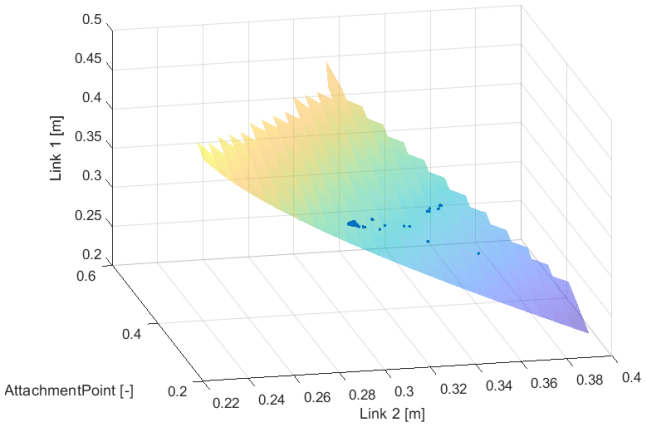

Fig. 14. Scatter plot of the solution space resulting from the optimization plotted in the search space

TABLE 4
Tested configurations for RRR and PRR cases in which **x** is the parameter vector $[L_1,\ L_2, AP]$ and **f** is the objective function vector with the respective objectives being 1) total link length 2) workspace 3) mean joint distance to body and 4) inverse of determinant jacobian the sensitivity is the sensitivity per objective function for a change of $1\ \%$ in link length

RRR				
x	$0.44\ [m]$	$0.36\ [m]$	$0.24\ [m]$	
f	$0.88\ [m]$	$1.00\ [-]$	$0.30\ [m]$	$1.20\ [-]$
Sensitivity	$0.5\ \%$	$0.8\ \%$	$1.9\ \%$	$3.9\ \%$
PRR				
x	$0.25\ [m]$	$0.36\ [m]$	$0.23\ [m]$	
f	$0.69\ [m]$	$1\ [-]$	$2.65e^{-3}\ [m]$	$2.08\ [-]$
Sensitivity	$3.7\ \%$	$0.5\ \%$	$9.3\ \%$	$9.5\ \%$

optimization the resulting link lengths are made and the corresponding joint types are attached. The shoulder is made such that it matches the misalignment model proposed in figure 2. The shoulder is then moved throughout its entire workspace. This is achieved by rotating it from $-85°$ to $85°$ and doing this for every shoulder translation within the range specified in the requirements in steps of $1\ [cm]$ for the vertical translation and for the minimum and maximum values for the horizontal translation. Videos are made which are further analysed. The analysis is performed by tracking the attachment point with kinovea software [21]. This path is plotted and the boundary of the theoretical workspace that should be reachable is plotted around it. The result is visually checked to determine whether the configuration achieves the full workspace.

The joint distance is verified by using the same test set up described before. The videos taken from this test are used. Markers are placed on the location of the middle joint and on the location of the hip and

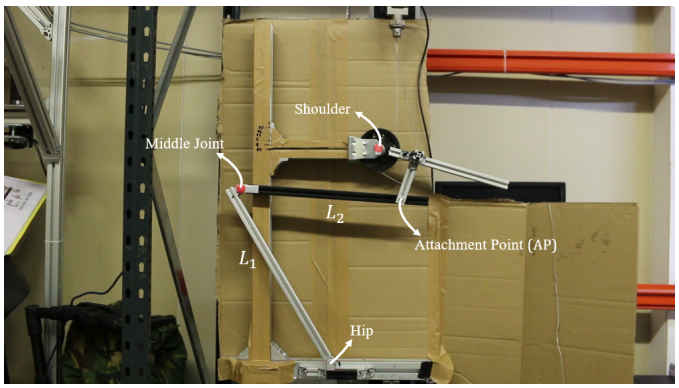

Fig. 15. Test setup of the RRR case with markers on the hip shoulder and the middle joint

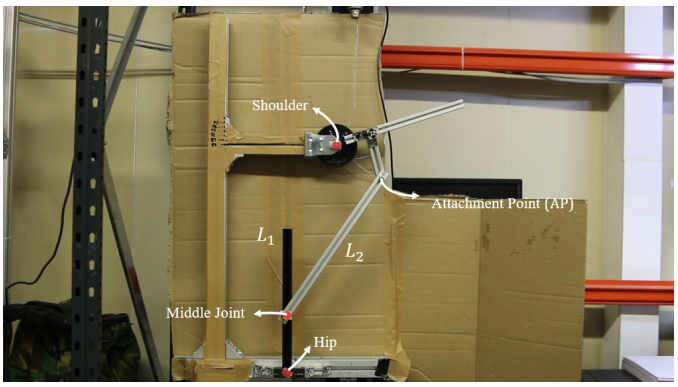

Fig. 16. Test setup of the PRR case with markers on the hip shoulder and the middle joint

the shoulder before performing the workspace test. `kinovea` is used to track the location of the marker on the moving joint. This data is used to compute the distance in pixels and converting the pixels to real dimensions by known dimensions on the video.

The singularity avoidance is not quantifiable from the video analysis since the optimization only gives the number of the determinant and this gives no information on the angle at which this value presented itself. The videos were analysed by eye to see if no singularities occured.

6 Test Setup

The test set up was made with aluminium profiles made by item24 [22]. These profiles were further adapted by hand to comply to the needs of the setup. The bars were sawn to the right size and holes were drilled to fit the joints. A pulley was connected to a tensile tester with a string to supply a torque on the shoulder joint which causes movement in the entire system. Markers were placed on the shoulder joint, the hip joint and the middle joint. Filming was done with a tripod and a Canon EOS 70D equipped with the $18-50mm$ kit lens. The RRR test setup is shown in figure 15 and the PRR test setup is shown in figure 16.

7 Validation Results

With the arm length assumed to be 0.35 $[m]$ the total link length for the RRR case is equal to $0.44 + 0.36 + 0.24 \cdot 0.35 = 0.88$ $[m]$ and for the PRR case this becomes $0.25 + 0.36 + 0.23 \cdot 0.35 = 0.69$ $[m]$

The second objective function is the workspace that exoskeleton can achieve as part of the workspace that the arm can achieve. These workspaces draw an area in cartesian space due to the fact that the arm can not only rotate but also translate. For both cases the full range of motion specified in the requirements should be achieved according to the optimization results. The video analysis proved that this was indeed the case for both of the configurations. Figure 17 shows the result of the attachment point tracking for the RRR case. This tracking path is plotted in the workspace area it should achieve as is used in the optimization process. Figure 17 shows the same results for the PRR case. The red dotted boundary shows the are that the attachment point should cover according to the used equations in the optimization. The blue solid lines represent the tracking results of the video analysis. The results in figure 17 and 17 show that not all tracking results finished the full stroke of $[-85°, 85°]$. This is due to the test being stopped earlier than the specified range or by stopping tracking too soon.

The third objective function is the joint distance. Video analysis showed that for the RRR case the average marker distance to the line from hip to shoulder over all 12 videos was 0.28 $[m]$. The results of the tracking is shown in figure 18. The PRR case showed a test outcome of 0.02 $[m]$, the tracking result is shown in figure 18. The test results from the joint distance comparison deviated from the optimization results by 7.4 $\%$ and 13 $\%$ for the RRR and the PRR case respectively. Furthermore the tracking software used is not perfectly accurate. This can be shown by figure 18. The PRR slider should run perfectly vertical, however figure 18 shows a deviation from this vertical line. The mean of maximum deviation from the vertical line over all 12 runs is around $3e^{-3}$ $[m]$. Which is 13 $\%$ of the PRR joint distance and 1.1 $\%$ of the RRR joint distance.

Also note that figure 18 shows a big shift horizontal shift, this is due to the camera being moved after the first six videos. This caused the test setup to be localized at a different position in the frame.

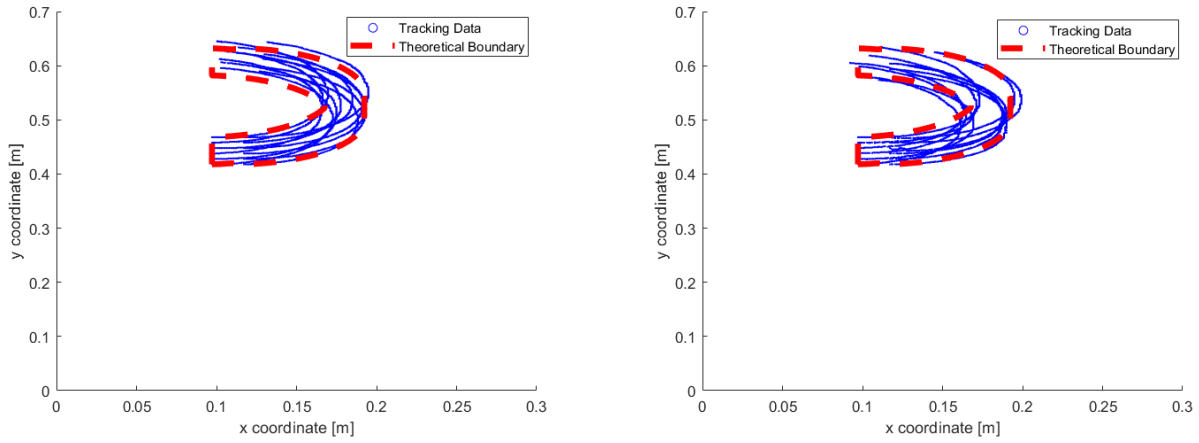

Fig. 17. Reachable workspace for the RRR case in figure (a) and the PRR case in figure (b) obtained by tracking the attachment point location and plotted this in the theoretical workspace area it should fill

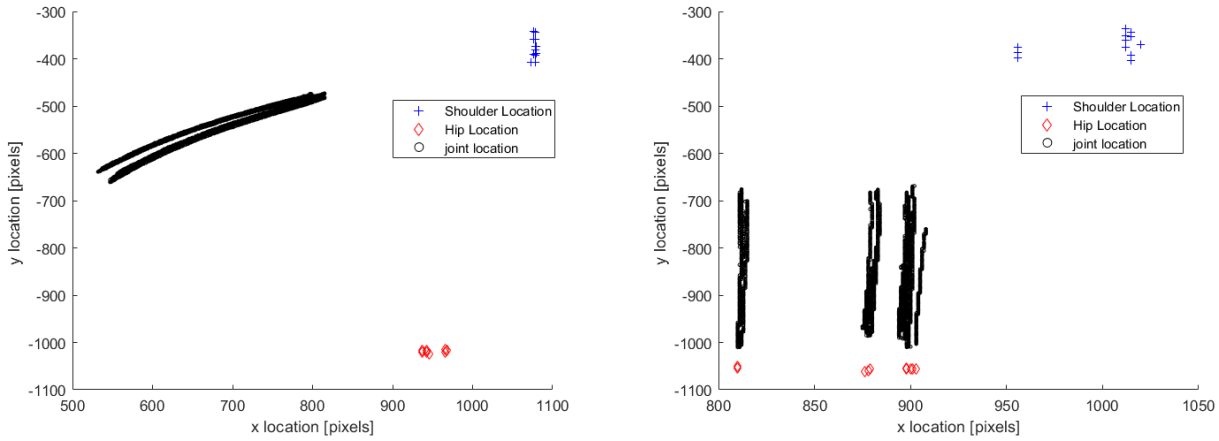

Fig. 18. Joint distance of the RRR case in figure (a) and the PRR case in figure (b) plotted in Cartesian space measured in pixels, the paths show the joint location of the middle joint and the right top circles show the shoulder locations and the left bottom show the hip locations

During the motion of both configurations no singularities occurred.

8 Discussion and Recommendations

A method is presented that provides a systematic way of self aligning exoskeletons with a pro active attitude towards ergonomics. The designer is offered an approach by which well informed design choices can be made and by which all design options are considered such that the designer is not left with a sub-optimal design. The method extends the mathematical tools to develop self aligning mechanisms proposed by Cempini [9].

The proposed method is meant for all exoskeleton applications but is only verified in a planar exoskeleton for the shoulder. The misalignment model on which the configurations are based can easily be altered to fit the human joint under investigation. The reasons of exclusion and the objectives for optimization are not dependent on the type of joint that is investigated. The generated link lengths are dependent on the user dimensions and have to be set up for each separate case. When making the move to three dimensions the degrees of freedom of the self aligning chain has to be at least equal to six. The amount of joint types that can be selected from also increases to six. This increases the amount of possibilities significantly.

The aid of a computer is used in the design process to cope with the large amount of possibilities. The proposed method uses optimization to help the designer make decisions by narrowing down

the solution space. This is currently the only part that is truly computer aided. The generation of configurations and the geometrical relations that define the search space for the optimization are now set up by hand. Future research could focus on automatically generating the configurations and the search space.

Note that the proposed method is meant as a guideline for ergonomic exoskeleton design. The vision is that exoskeletons can be designed with a certain base level of ergonomic performance. The approach can be extended upon by adding more knowledge that is gathered in the future. Currently only the kinematic part is considered and future research could focus on the kinetic part as well. Force is an important factor in ergonomics and should be accounted for. Additions like minimizing shear forces and minimizing actuator demands are examples of such factors. Furthermore the current optimization uses relatively simple metrics. The distance to the body is now determined by taking the distance of the middle joint to the line that runs from the hip to the shoulder. This metric could be made more realistic by adding a non-linear function that represents the human body. Also the distance from the rigid bodies to this ”body” can be taken instead of the joint distance. One could also think of adding boundaries to the system which it is not allowed to exceed during motion. Singularity avoidance is now performed by the determinant of the jacobian, however the condition number could also be used. This would not only detect singularities but also give an indication of how close the system is to one [23].

The results for the optimization showed a large spread in the objective space for the RRR case and a more clustered results for the PRR case. An explanation for this could be that the RRR objective space shows more minima with around the same value and the PRR objective space has some more dominant minima to which the algorithm converges faster. This spread is also present in the solution space and means that more variety is design is possible for the RRR case compared to the PRR case.

The results also showed inaccuracies in the workspace area. This is caused by the `areaintersect` function that was used. This function was set on a resolution of 400. For more accurate results this could be further increased, however increasing the resolution drastically increases the time the optimization algorithm takes to complete. The chosen resolution was a trade-off between time and accuracy.

The test results show deviations from the optimization results. These differences can be explained: First of all the sensitivity of a change in joint distance for a change in 1 % of one of the link lengths was found te be 1.9 % and 9.4 % for the RRR case and the PRR case respectively. The test setup was made by hand and inaccuracies of 1 % in link lengths are likely to be present. Together with the inaccuracy of the tracking software used the differences are within acceptable bounds.

The proposed method could serve as a tool that is used as the new standard in exoskeleton design. A tool by which it is made sure that ergonomics is systematically addressed and design choices can be well funded.

9 Conclusion

A method for designing self aligning exoskeletons has been expanded by a synthesis approach in combination with an optimization based on ergonomic objectives, hereby creating a systematic way of developing self aligning exoskeletons whilst taking ergonomics into account. The proposed method is based on self aligning mechanism theory and is heavily focused on ergonomics. The proposed approach consist of determining the possible joint configurations based on self aligning mechanism theory. The designer can choose from six kinematic pairs to configure in three dimensions and two in two dimensions. After synthesis of the configurations these configurations can be narrowed down according to kinematic requirements. Within the remaining set the physically feasible link length combinations for the specific joint configurations are obtained by geometric relations. These physically feasible sets are the bounds of an optimization in which ergonomic factors are optimized. The proposed method is applied to a two dimensional case of a passive shoulder exoskeleton. In this application the initial analysis left three configurations: RRR, RPR and PRR. The physically possible set of link lengths connecting these joints was determined. The found set served as the constraints of the optimization problem. This paper optimized the total link length of the exoskeleton, the preservation of the range of motion of the combined system of human and machine, the distance to the body was minimized and singularities were avoided. The test results validated the application of the proposed method in two dimensions. The proposed method can be applied in three dimensions as well although this increases the amount of options significantly. Efforts should be made to expand the proposed method in three dimensions.

References

[1] E. Guizzo and H. Goldstein, “The rise of the body bots,” *IEEE Spectrum*, vol. 42, no. 10, pp. 50–56, 2005.

[2] "Exoskeleton Report." [Online]. Available: https://exoskeletonreport.com/what-is-an-exoskeleton/
[3] N. V. Dijk, "Wearable Passive Upper Extremity Exoskeletons for the Shoulder : A Review," pp. 1–7.
[4] W. Karwowski, "Ergonomics and human factors: The paradigms for science, engineering, design, technology and management of human-compatible systems," *Ergonomics*, vol. 48, no. 5, pp. 436–463, 2005.
[5] A. Schiele, *Fundamentals of ergonomic exoskeleton robots*, 2008. [Online]. Available: http://www.narcis.nl/publication/RecordID/oai:tudelft.nl:uuid:80d212ff-37d0-4ddd-aee1-820bb24cf35e
[6] N. Jarrassé and G. Morel, "A methodology to design kinematics of fixations between an orthosis and a human member," *IEEE/ASME International Conference on Advanced Intelligent Mechatronics, AIM*, pp. 1958–1963, 2009.
[7] A. Schiele and F. C. T. Van Der Helm, "Kinematic design to improve ergonomics in human machine interaction," *IEEE Transactions on Neural Systems and Rehabilitation Engineering*, vol. 14, no. 4, pp. 456–469, 2006.
[8] A. H. Stienen, E. E. Hekman, F. C. Van Der Helm, and H. Van Der Kooij, "Short Papers of Joint Rotations and Translations," vol. 25, no. 3, pp. 628–633, 2009.
[9] M. Cempini, S. M. M. De Rossi, T. Lenzi, N. Vitiello, and M. C. Carrozza, "Self-alignment mechanisms for assistive wearable robots: A kinetostatic compatibility method," *IEEE Transactions on Robotics*, vol. 29, no. 1, pp. 236–250, 2013.
[10] M. Cempini, M. Cortese, and N. Vitiello, "A powered finger-thumb wearable hand exoskeleton with self-aligning joint axes," *IEEE/ASME Transactions on Mechatronics*, vol. 20, no. 2, pp. 705–716, 2015.
[11] H. C. Hsieh, D. F. Chen, L. Chien, and C. C. Lan, "Design of a Parallel Actuated Exoskeleton for Adaptive and Safe Robotic Shoulder Rehabilitation," *IEEE/ASME Transactions on Mechatronics*, vol. 22, no. 5, pp. 2034–2045, 2017.
[12] M. Cenciarini and A. M. Dollar, "Biomechanical considerations in the design of lower limb exoskeletons," *IEEE International Conference on Rehabilitation Robotics*, pp. 10–14, 2011.
[13] A. K. Mallik, A. Ghosh, and G. Dittrich, *Kinematic Analysis and Synthesis of Mechanisms*, 1994.
[14] E. N. Marieb and K. Hoehn, *Human Anatomy & Physiology*, 2007, vol. 7.
[15] K. J. Waldron, G. L. Kinzel, and S. K. Agrawal, *Kinematics, Dynamics, and Design of Machinery*, 3rd ed. John Wiley & Sons, 2016.
[16] A. Abraham, L. Jain, and R. Goldberg, *Evolutionary Multiobjective Optimization*, 2005. [Online]. Available: http://medcontent.metapress.com/index/A65RM03P4874243N.pdf
[17] P. Scott, Kazutaka Kogi, and B. McPhee, *Ergonomics Guidelines for occupational health practice in industrially developing countries*, 2010.
[18] "Dined." [Online]. Available: https://dined.io.tudelft.nl/en/database/introduction
[19] A. C. Lukasiewicz, P. McClure, L. Michener, N. Pratt, B. Sennett, P. Ludewig, A. C. Lukasiewicz, P. McClure, L. Michener, N. Pratt, and B. Sennett, "Comparison of 3-Dimensional Scapular Position and Orientation Between Subjects With and Without Shoulder Impingement," *Journal of Orthopaedic & Sports Physical Therapy*, vol. 29, no. 10, pp. 574–586, 1999. [Online]. Available: http://www.jospt.org/doi/10.2519/jospt.1999.29.10.574
[20] H. Graichen, S. Hinterwimmer, R. Von Eisenhart-Rothe, T. Vogl, K. H. Englmeier, F. Eckstein, D. Harryman, J. Sidles, J. Clark, K. McQuade, T. Gibb, and F. Matsen, "Translation of the humeral head with passive glenohumeral on the glenoid motion," *Journal of Biomechanics*, vol. 38, no. 4, pp. 1334–1343, 2005.
[21] "Kinovea." [Online]. Available: https://www.kinovea.org/
[22] "Item 24." [Online]. Available: http://www.item24.nl/
[23] R. M. Corless and N. Fillion, *A graduate introduction to numerical methods: From the viewpoint of backward error analysis*, 2013.

4

Force-Deflection Behaviour

In chapter 3 a method has been proposed by which the ergonomics of exoskeletons can be designed in a systematic way. The focus of the chapter was the kinematic aspect. However in ergonomics the interaction forces play a large role as well. Avoiding shear forces and high pressures on the skin is important since they can cause discomfort or injury [42]. The focus of this thesis in on passive exoskeletons. These passive exoskeletons do not need batteries for their functioning and can be used for unlimited time. In chapter 2 it is shown that multiple of these passive devices exist and recent efforts have been made to make the passive exoskeletons from compliant mechanisms [7, 10, 16, 20]. Compliant mechanism have a number of advantages over rigid bodies: they offer a low weight and allow for compact design with fewer moving parts. Energy is stored in bending elements and this results in less energy loss due to friction [15]. The purpose of this chapter is to create a step towards a compliant exoskeleton by using the results from chapter 3 as the basis for the kinematic structure. The vision is that by using this structure which is based on self aligning mechanisms and ergonomic guidelines the resulting compliant mechanisms will keep some of these characteristics.

First the general approach that is taken to move towards a compliant mechanism is presented. The design approach from chapter 3 is extended by the approach to move towards a compliant mechanism. And steps are made to apply this to the same case as was done in chapter 3.

4.1. Compliant Mechanisms

Although compliant mechanisms have numerous advantages they also present challenges of which one is that the energy storage is done by deflection of material, this results in very non-linear relations. One way of tackling this is by the pseudo rigid body model (PBRM) [41]. This approach can be seen as an in between step from rigid bodies to compliant mechanisms. A pseudo rigid body model assumes the joints of the rigid bodies to have a stiffness and hereby lumping the compliancy of the structure to one point. An example of such a pseudo rigid body model is given in figure 4.1.

The pseudo rigid body model is a method that describes the force-deflection behaviour of a compliant mechanism by using lumped compliancy. In a later stage distributed compliancy is added with the same force-deflection behaviour as the PBRM prescribes. This can be applied to exoskeletons by adding stiffness to the joints that connect the rigid bodies, this will add the lumped compliancy. The stiffness of the joints required to provide the desired force-deflection behaviour is determined. In a later stage this compliancy is distributed. The desired support is determined by the change in energy V that is needed to provide this support. This change in energy needs to be equal to the change in potential energy in the joints with stiffness k. It can be stated that the potential energy in a rotational spring with stiffness k is equal to:

$$U = \frac{1}{2} \cdot k \cdot \theta^2 \tag{4.1}$$

In which U is the potential energy, k is the stiffness and theta is the deflection of the angle. By modelling the human joint as a spring this changes to:

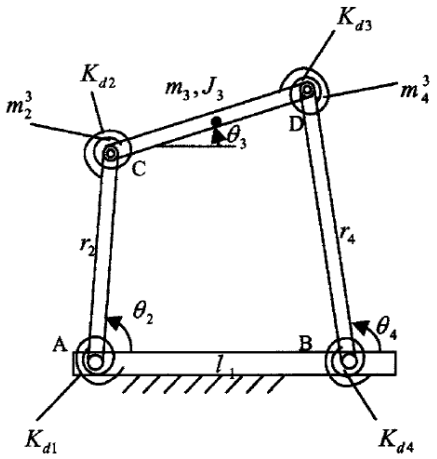

Figure 4.1: Example of a four bar pseudo rigid body model in which the hinges are modelled with a stiffness, adapted from [41]

$$U_{joint} = \frac{1}{2} \cdot k_{joint} \cdot \theta_{joint}^2 \tag{4.2}$$

The change in this potential energy should be the change in the total energy V that is required for the desired support. To determine the change in potential energy equation 4.2 is differentiated w.r.t. θ_{joint}.

$$\frac{dU_{joint}}{d\theta_{joint}} = k \cdot \theta_{joint} = M_{joint} \tag{4.3}$$

In which M_{joint} is the resulting moment force in that joint. Using the fact that the change in total energy for providing the desired support is equal to the change in potential energy in the supporting joint: $dV = dU_{joint}$ and rearranging equation 4.3 the following is obtained:

$$dV = M_{joint} \cdot d\theta_{joint} \tag{4.4}$$

This states that the required change in energy is equal to the moment present in the joint multiplied by the change in joint angle. For prismatic joints the same relations are used but the moment M_{joint} is then substituted by the force in the joint F_{joint} and the joint angle θ_{joint} is substituted by the joint displacement ϵ_{joint}. This results in an exoskeleton with a lumped compliancy by which the force-displacement behaviour can be described . This provides a basis for determining an exoskeleton with distributed compliancy.

4.2. Extended Design Approach

The result from the paper in chapter 3 is a self aligning mechanism. This mechanism is a combination of rigid bodies connected with joint and serves as a good basis for a PBRM. To move towards the creation of a self aligning compliant mechanism the design approach presented in chapter 3 can be extended as shown in figure 4.2. The result of the optimization is a Pareto front of optimal solutions. Within this set a decision has to be made on the fittest solutions for a particular application. This can be done by designer choice or by computational methods. The next step is to add stiffness to the joints after which the same force-deflection behaviour can be obtained by distributing the compliance over the entire structure.

The dark boxes will be applied to the passive upper extremity exoskeleton for the shoulder, as done in chapter 3. The greyed out boxes will not be discussed in this thesis.

4.3. Application to a Passive Upper Extremity Exoskeleton for the Shoulder

This section applies the proposed force behaviour method to the same case as chapter 3 does. The same assumptions on dimensions are made as in chapter 3. The optimization results obtained in chapter 3 are used in the force-deflection behaviour analysis of this exoskeleton.

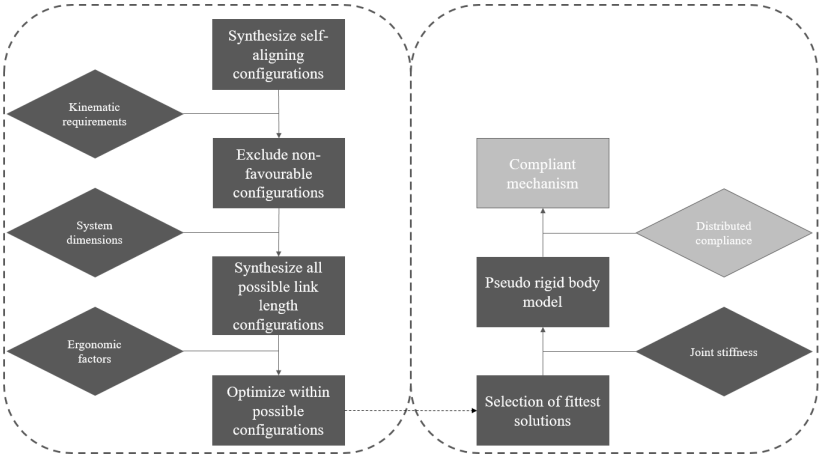

Figure 4.2: The design flow chart from chapter 3 presented in the left box with the extend approach leading to a self aligning compliant mechanism in the right box

4.3.1. Selection of Fittest Solutions

After the kinematic synthesis the designer is left with a set of Pareto optimal solutions. A decision has to be made to determine the solutions that are used for the force-deflection analysis. This section describes the method of decision making.

After the optimization the designer is left with a set of Pareto optimal solutions. This set is still quite large (77 solutions for the RRR case and 90 solutions for the PRR case) and to make a decision on the most promising solutions use is made of computational methods. To do this the Utopia point [24] is used. The Utopia point is a point for which all objective functions are minimized [24]. This point does not lie within the feasible set and lies outside of the Pareto front. The closest point on the Pareto front should theoretically be the best solution as illustrated by figure 4.3.

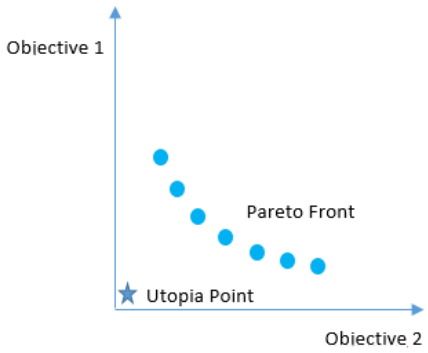

Figure 4.3: Graphical representation of a two dimensional Pareto front and the corresponding utopia point which lies outside of this front but minimizes all objectives

The second measure used is the sensitivity to uncertainties which is further elaborated upon in appendix D. A threshold is set on the allowed sensitivity as a measure for robustness. For the selection of the fittest solutions the ones closest to this utopia point below the proposed threshold are chosen.

For the four objectives used in this application the best solutions are 0 $[m]$ for the total link length since the ideal minimum for the link length is 0 $[m]$. The workspace is expressed as the achievable workspace of the entire system as part of the arm workspace. In the optimization the inverse of this relation is used which has a minimum value of 1 $[-]$. The joint distance ideally is 0 $[m]$ to the human body throughout the entire

workspace. The minimum achievable value is 0 [−] for the singularity avoidance. this results in the utopia point: $x_u = [0,1,0,0]$

To provide a fair comparison of distance first all objective values are normalized based on their maximum value and the utopia point as is done by Marler [24] so:

$$f_{ij,normalized} = \frac{f_j(x_i) - f_j(x_u)}{max(f_j) - f_j(x_u)} \tag{4.5}$$

Where subscript i denotes the i^{th} optimal point and j denotes the objective number out of the four resulting objectives.The range of the normalized fitness will lie between $[0,1]$ depending on the accuracy of the results now the distance is determined by taking the 2-norm of the objective vector:

$$d_{utopia} = ||\mathbf{f}_i||_2 \tag{4.6}$$

The minimum of this set of distances will give the point closest to the Utopia point. In this application a comparison between multiple solutions is desired. This gives an insight in the force-deflection behaviour of different cases. For this reason five points are selected from the solution space.

The maximum sensitivity for the RRR case to an uncertainty of 1 % in link length is plotted as a function of the distance to the Utopia point in figure 4.4a. A sensitivity of 7 % is chosen as a threshold. When decreasing the threshold to 5 % the average distance of the first five points to the utopia point increased from 1.12 [−] to 1.17 [−]. The same relation is plotted in figure 4.4b for the PRR case. In this case the sensitivity threshold has been set to 5 % since this implied no difference in the average distance to the utopia for the first five points.

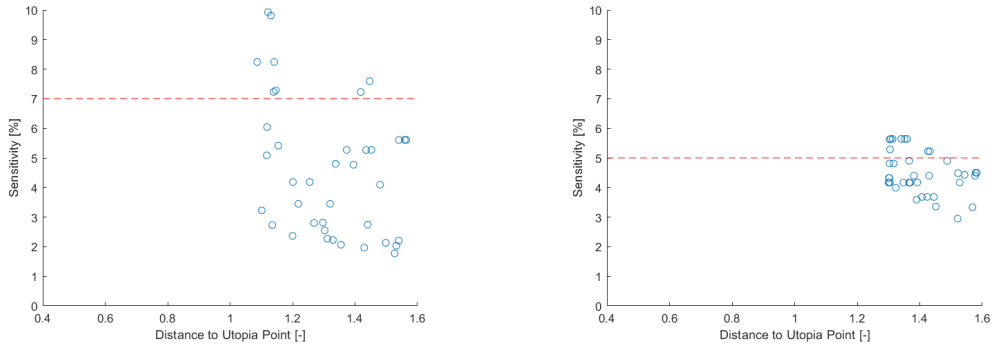

(a) (b)

Figure 4.4: Maximum sensitivity to an uncertainty of 1 % in link length is plotted as a function of the distance to the utopia point for the RRR case in figure 4.4a and for the PRR case in figure 4.4b , the dotted line represents the sensitivity threshold

The link lengths of the five fittest points that result from this analysis are shown in table 4.1. Again clustering in the PRR results is observed as the PRR configurations lie very close to each other.

4.4. Pseudo Rigid Body Model

Stiffnes is now added to the exoskeleton configurations resulting from the optimization. In this analysis stiffness is only added to one joint at a time. Furthermore no stiffness is added to the joint at the attachment point (AP) location since little room is present here for spring parts due to the human arm. This results in four possible configurations: $\bar{R}RR$, $R\bar{R}R$, $\bar{P}RR$ and $P\bar{R}R$ in which the bar indicates a joint with stiffness. The two configurations for the RRR case are shown in figure 4.5 and for the PRR case in figure 4.6.

To determine the required stiffness of each joint the change in energy for the desired support has to be determined. The purpose of this application is to balance the weight of the arms. The energy needed to provide the right amount of support is equal to the potential energy of the arms. The potential energy is determined done by the simple relation:

Table 4.1: Link length configurations of fittest points resulting from the performed analysis

RRR	Link One [m]	Link Two [m]	Attachment Point [-]
	0.41	0.32	0.2989
	0.44	0.36	0.2354
	0.44	0.41	0.3119
	0.66	0.40	0.2831
	0.71	0.43	0.2870
PRR	0.28	0.39	0.2007
	0.28	0.39	0.20
	0.28	0.39	0.20
	0.28	0.39	0.20
	0.28	0.39	0.20

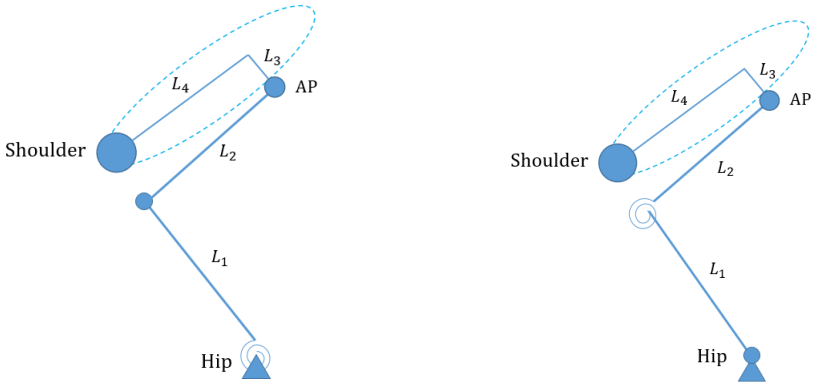

(a) $\bar{R}RR$ (b) $R\bar{R}R$

Figure 4.5: Pseudo rigid body model of the RRR configuration

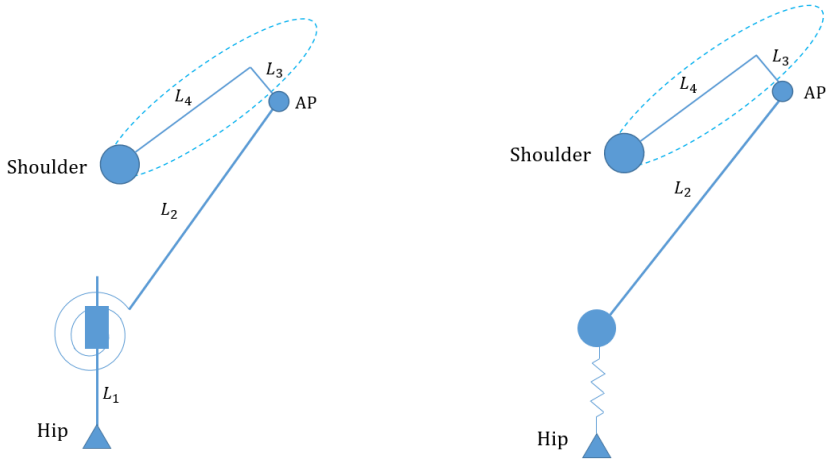

(a) $P\bar{R}R$ (b) $\bar{P}RR$

Figure 4.6: Pseudo rigid body model of the PRR configuration

$$V_{arm} = m_{arm} \cdot g \cdot h_{arm} \tag{4.7}$$

Where V_{arm} is the potential energy of the arm, m_{arm} is the mass of the arm, g is the gravitational acceleration which is assumed to be 9.81 $[\frac{m}{s^2}]$ and h_{arm} is the height of the centre of mass (CoM) of the arm. The height is taken to be 0 when the arms are hanging along the side of the body and then increases by:

$$h_{arm} = CoM_{arm} - cos(\theta_{arm}) \cdot CoM_{arm} \tag{4.8}$$

This can be done for both upper and forearm and their sum is the total potential energy of the system assuming the exoskeleton attached to be massless.

$$V_{total} = V_{upperarm} + V_{lowerarm} \tag{4.9}$$

To determine this total energy the weight of the upper arm arm is assumed to be 2.8 % of the total body mass and the weight of the forearm is assume to be 1.6 % of the total body mass [8, 40]. With the total body mass in the Netherlands being 84 $[kg]$ for the average male [3] this results in a mass of 2.4 $[kg]$ for the upper arm and 1.3 $[kg]$ for the forearm. The centre of mass of the upper arm is located at 45 % of the segment length measured from the proximal side of the arm. For the forearm this is 42 % [8, 40]. With these assumptions the energy curve presented in figure 4.7 is obtained.

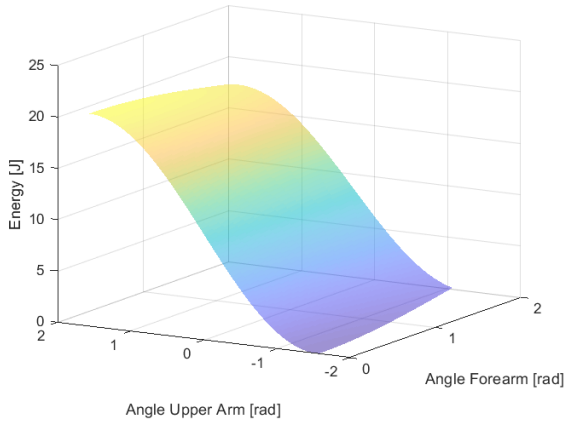

Figure 4.7: Potential energy as a function of the upper arm angle and the forearm angle with an upper arm weight of 2.4 $[kg]$ a forearm weight of 1.3 $[kg]$

As can be seen from both equation 4.9 and figure 4.7 the total potential energy is dependent on both the upper and forearm angle. These two are dependent on each other since the forearm angle changes w.r.t. the horizontal axis when the upper angle changes. In this analysis the least demanding position of the forearm is used which is π $[rad]$ w.r.t. the upper arm.

To further analyse the joint movement relation with the human joint movement use is made of a multi body dynamics model. To make this model in `MATLAB` the TMT method is used [31]. With this model the joint angles of each configuration can be shown as a function of the upper arm angle. Furthermore equation 4.4 can be rewritten as:

$$M_{joint} = \frac{dV_{total}}{d\theta_{joint}} \tag{4.10}$$

With this relation the moment of the joint can be computed as a function of the upper arm and hence the required moment/force deflection curve can be determined that is needed to provide balancing. The moment curves for all five configurations are determined for an upper arm angle of $[-85°, 85°]$ at a shoulder location of $[x_{shoulder}, y_{shoulder}] = [0.1\ m, 0.5\ m]$. The moment curves with respect to the joint angle for all five configurations are shown in figure 4.8 for all configurations of the RRR case and figure 4.9 for the PRR case.

In figures 4.8 and 4.9 two lines can be seen in most plots: a blue and a red one. The red line indicates that a positive movement (counter-clockwise) in the shoulder joints results in negative movement (clockwise or vertically downwards in the PRR configuration) in the joint. This also causes vertical asymptotes in the graphs due to the fact that a change in arm angle causes an infinitely small change in joint angle. In this case infinite stiffness is needed to provide the change in energy required for balancing. Furthermore It can be seen that certain regions have a quasi linear stiffness profile.

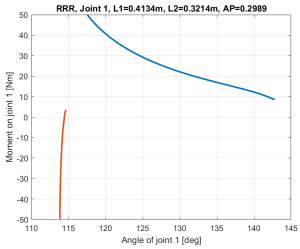

(a)

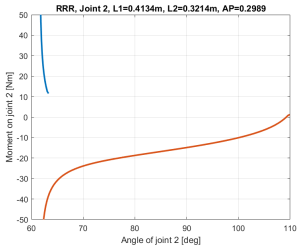

(b)

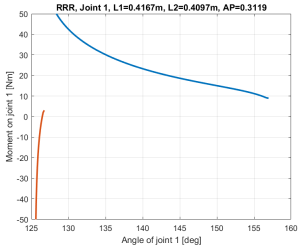

(c)

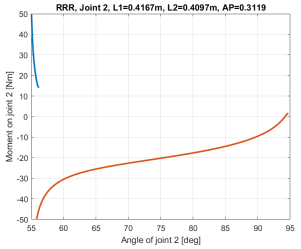

(d)

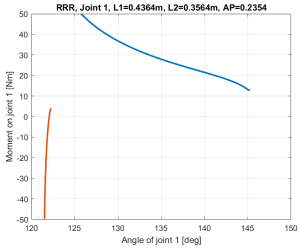

(e)

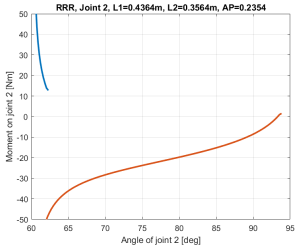

(f)

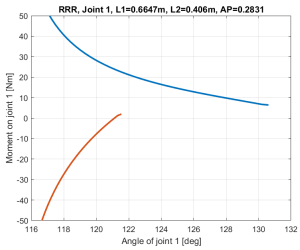

(g)

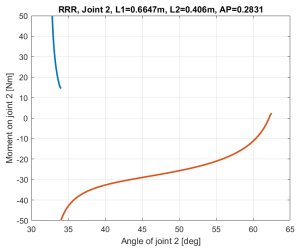

(h)

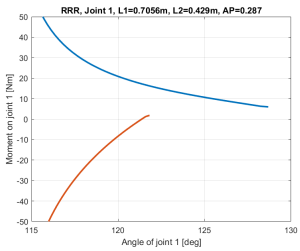

(i)

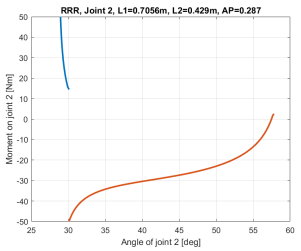

(j)

Figure 4.8: stiffness profile of the RRR case with respect to the joint angle measured from the horizontal x-axis for the entire range of the upper arm angle: $[-85°, 85°]$

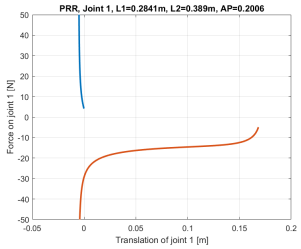

(a)

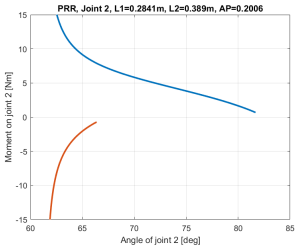

(b)

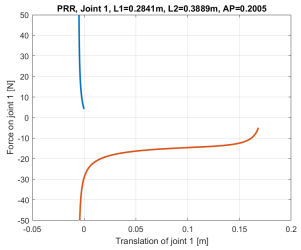

(c)

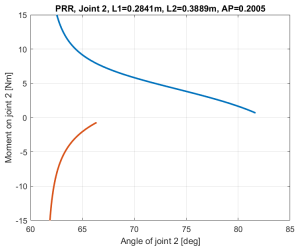

(d)

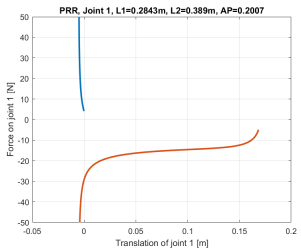

(e)

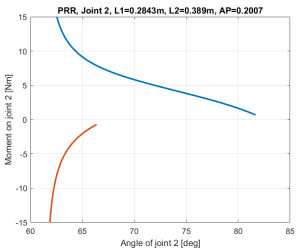

(f)

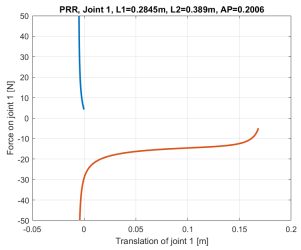

(g)

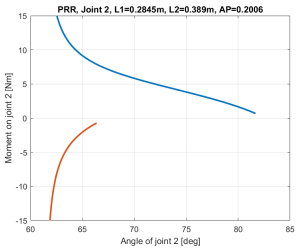

(h)

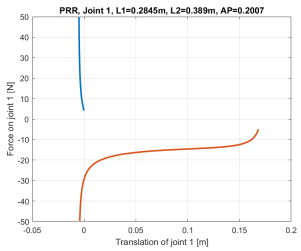

(i)

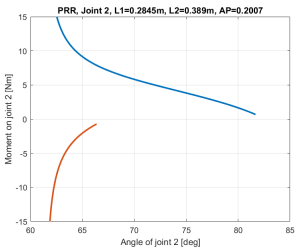

(j)

Figure 4.9: stiffness profile of the PRR case with respect to the joint angle measured from the horizontal x-axis for the entire range of the upper arm angle: $[-85°, 85°]$

5

Discussion and Recommendations

The state-of-the-art of upper extremity passive exoskeletons for the shoulder was investigated and a method is proposed which uses a systematic approach to create self aligning exoskeletons with use of ergonomic guidelines. This approach was extended by creating a pseudo rigid body model which is a step closer to the vision of the design of a self aligning compliant mechanism.

None of the state-of-the-art exoskeletons show two or more prismatic joints in their design. This is in line with the choice to exclude P-heavy configurations. What is also interesting to see is that the configurations that result from the application of the proposed method are different than the configurations seen in the current state-of-the-art. This shows that the design approach taken leads to different concepts and designs than the ones obtained with currently existing design approaches. To see whether the resulting design performs better than the state-of-the-art a comparative effectiveness study should be performed to validate this. An interesting observation is that there are configurations present in the state-of-the-art that have a prismatic joint at the arm. During the application of the proposed method a prismatic joint at the arm required a range that exceeded the length of the arm and were excluded. A reason for this difference is the presence of more than three degrees of freedom in the planar perspective. This will limit the required range on the prismatic joint. Another reason is that the attachment of the exoskeleton is closer to the shoulder instead of the hip. This also lowers the demands on the range of the prismatic joint.

In the selection of the fittest solutions the Utopia point is used. Which makes use of the singularity avoidance, however the value of the determinant does not indicate a better or worse solution. In future applications either the condition number should be used since this would indicate the closeness to a singular position or the utopia point has to be evaluated for just the first three objectives.

The proposed method in chapter 3 only considered the kinematic behaviour. This was extended upon in chapter 4 with a force analysis by adding stiffness to the joints. This was done with the help of Bas Wagemaker. The resulting models showed quasi linear stiffness profiles in multiple solution points for a limited range of motion. The magnitude of the moments are achievable with normal springs, however they might prove to be challenging in compliant mechanism design. In future applications of this method force behaviour could be implemented into the optimization process to account for interaction forces on the human-machine interface and to optimize for a desired stiffness profile to further comply to the ergonomic guidelines provided in chapter 3. Another challenge that can be identified is the change of joint position with a change in centre of rotation of the human joint. This behaviour will always lead to a force in case of stiff joints. For a self aligning mechanism this change of the centre of rotation of the human joint should be freely adaptable. Furthermore in this thesis the force behaviour was not validated by an experiment. This validation should be performed in future work.

The future vision is to create a self aligning compliant mechanism. By adding stiffness to the joints and prescribing the desired force-displacement behaviour a step in the right direction is made. The results of the analysis prove to be achievable and if the mentioned challenges are overcome this vision might become reality.

6

Conclusion

The state-of-the-art of wearable upper extremity exoskeletons for the shoulder was investigated. 11 devices were found. All of these devices have the same goal: to prevent musculoskeletal disorders. It is found that the state-of-the-art has a low focus on ergonomics and that little research is done in the effectiveness of these devices. A new method that systematically synthesizes and optimizes exoskeleton kinematics is proposed. This method is based on ergonomic guidelines and self aligning mechanisms. First, all possible joint configurations are synthesized on the basis existing theory for self aligning mechanisms. A portion of these configurations is then excluded. For the resulting set of configurations all possible link length configurations are generated. These results are used as the bounds for an optimization problem. The objectives of the optimization are based on ergonomic guidelines.

The method was successfully applied to a planar passive exoskeleton that aims on supporting the arms during labour activities. The optimization optimized three parameters: the first two link lengths and the attachment point to the human arm by means of four objective functions. These objective functions considered maximizing the shared workspace of human and machine, minimizing the distance of the machine to the human body throughout the entire motion, keeping the total link length as small as possible and by avoiding singular positions. This method was verified with a simple model that showed the correctness of the outcome of the optimization and verified the kinematic feasibility of the structure.

The verification was performed by video analysis and tracking. This tracking was done on the joints and the part of the prototype that resembled the human arm. The workspace was visually verified by tracking a point on the modelled arm and plot the tracking results in the theoretical workspace boundary. The Joint Distance was verified by taking the mean of the tracker distance to the body. With the tracker placed on the corresponding joint used in the objective function. The results were acceptable and prove that the used method is correct for the application to a planar exoskeleton for the shoulder.

The bridge to a compliant exoskeleton was then made by taking the results of the optimization and using this as the starting point for a pseudo rigid body model approach in which the required stiffness of each joint required to balance the upper arm was investigated.

A

Application to Shoulder Exoskeleton: Location and Configuration selection

This section elaborates on the choice of exoskeleton location and gives a more detailed insight in the generated configurations.

A.1. Location selection

The purpose for this application is to prevent musculoskeletal disorders. The sectors exposed most frequent to risk factors that cause these disorders are construction and industry [26]. This is were the exoskeleton will mainly be used. Working activities vary a lot. Hence effort is made to keep the exoskeleton compact and certain zones of the human body have to be kept free of material. This section describes where material can be present and where it can not. First of all no material should be present around the legs since this would hinder walking. Furthermore no material should be added around the butt, this will hinder the person wearing it from sitting down whilst wearing the device. Furthermore no material should be present around the head since this limits head movement. No material should be added in front of the upper body and the hips, this will limit the subject in standing closer to objects. Finally no material is added between the arms and the upper body, this will get in the way of letting the arms rest beside the body. These requirements result in the excluded zones shown in figure A.1.

The choice was made to secure the exoskeleton on the hip and make the connection from hip to arm to provide support to the upper arm. This choice was based on figure A.1 and the fact that the hip provides a solid basis for transferring forces.

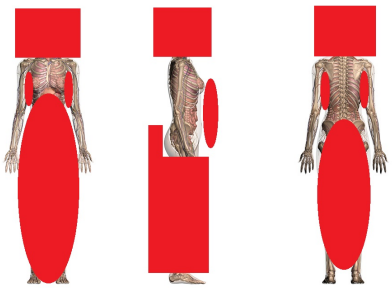

Figure A.1: Excluded material zones for exoskeleton according to ergonomic assumptions and working activities

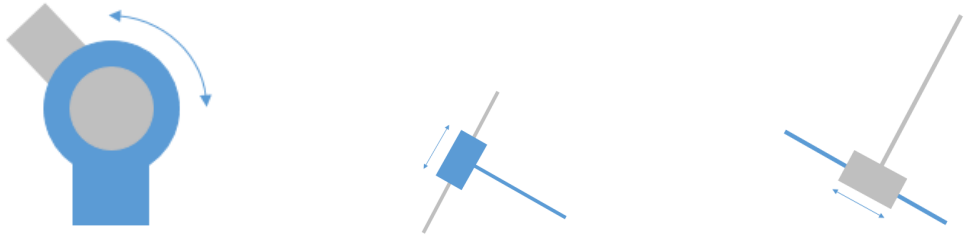

(a) (b) (c)

Figure A.2: Graphical representation of the three joint type options which add a degree of freedom in the planar case a) revolute joint b) slider joint option one c) slider joint option 2

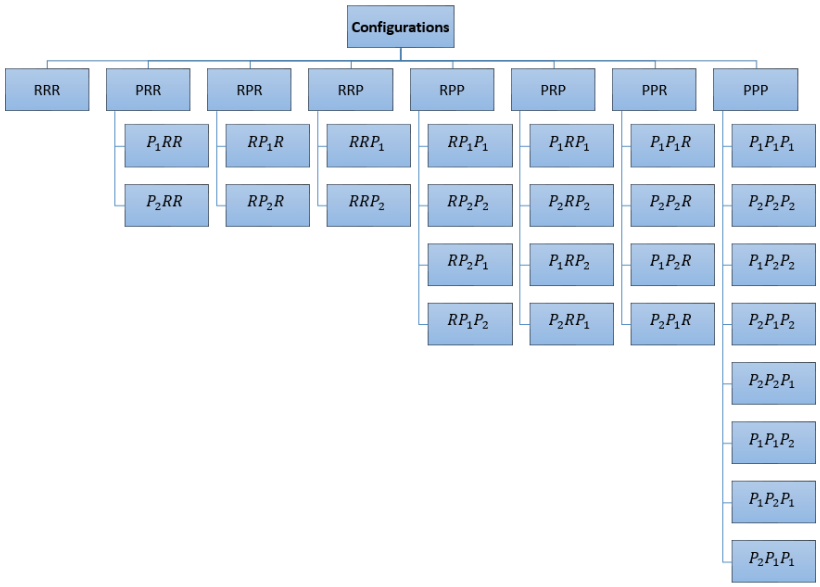

Figure A.3: Tree of all theoretically possible configurations when connection three joints in series in the planar case

A.2. Generated Configurations

In the planar case two types of joints can be used to add degrees of freedom to the system. A revolute joint as shown in figure A.2a and a slider joint as shown in figure A.2b and figure A.2c. Note that the slider can be configured in two different ways: blue slides over grey and grey slides over blue. Three of these joints have to be added to a system which results in $3^3 = 27$ options.

If for the revolute joint the denotation R is used and for a slider joint the denotation P (prismatic) a tree can be made that represents all the 27 possible configurations. This tree is shown in figure A.3. In which the subscript 1 or 2 on the P denotation stands for the two slider options mentioned previously.

B

Application to Shoulder Exoskeleton: Link Length Synthesis

This section provides a more detailed insight in the generation of all possible link lengths. Each configuration is addressed separately. The geometric relations that were used to derive the feasible set of link lengths are presented. This possible set of link lengths is generated under the assumption that the links have to stay connected and can not elongate. After the defining the geometric relations the results and the linear approximations of these results are shown.

B.1. Geometric Relations

The entire system under investigation can be split up in two parts: The human and the exoskeleton. The exoskeleton starts at the hip and in this application the human arm starts at the shoulder. The two systems meet at the attachment point (AP). These two systems have to stay connected throughout the entire motion. A graphical representation is shown in figure B.1.

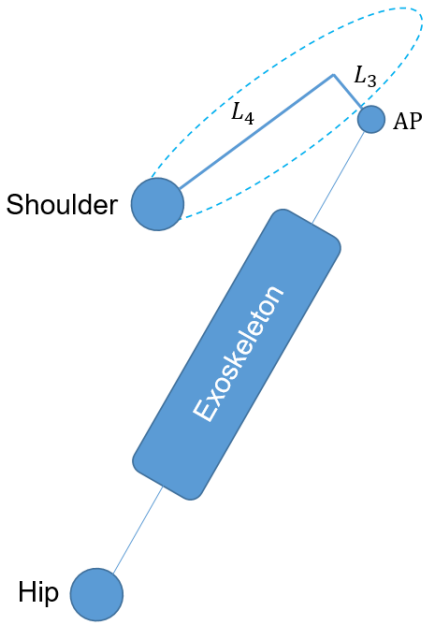

Figure B.1: Schematic representation of the system with the shoulder and the hip connected by an exoskeleton, the exoskeleton and the arm meet at the attachment point (AP)

The human arm is the same for every exoskeleton configuration, except for the RPR case (this will be explained later in this section). The location of the AP can be described in terms of the human joint angles, L_3 and L_4. The governing equations are presented by the hand of figure B.2. The AP can be represented as follows:

$$x_{AP} = x_{shoulder} + L_4 \cdot cos(q_3) + L_3 \cdot cos(q_3 - \frac{\pi}{2}) \tag{B.1}$$

$$y_{AP} = y_{shoulder} + L_4 \cdot sin(q_3) + L_3 \cdot sin(q_3 - \frac{\pi}{2}) \tag{B.2}$$

In which $[x_{AP}, y_{AP}]$ are the attachment point coordinates, $[x_{shoulder}, y_{shoulder}]$ are the shoulder coordinates, L_3 is the distance form the attachment point to the human skeleton, L_4 is the distance from the human shoulder to L_3 and q_3 is the angle describing the orientation of the human arm measured from the horizontal axis where counter-clockwise is positive.

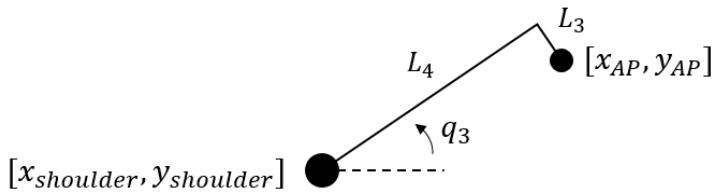

Figure B.2: Geometric model of the arm in which AP is the attachment point where the exoskeleton and the human arm meet, L_3 is the length between the human skeleton and AP and L_4 is the distance to the line representing L_3

B.1.1. RRR

The AP can also be described as a function of exoskeleton coordinates and dimensions. For the RRR case these relations are explained by figure B.3 and are defined as follows:

$$x_1 = x_{hip} + L_1 \cdot cos(q_1) \tag{B.3}$$

$$y_1 = y_{hip} + L_1 \cdot sin(q_1) \tag{B.4}$$

$$x_{AP} = x_1 + L_2 \cdot cos(q_2) \tag{B.5}$$

$$y_{AP} = y_1 + L_2 \cdot sin(q_2) \tag{B.6}$$

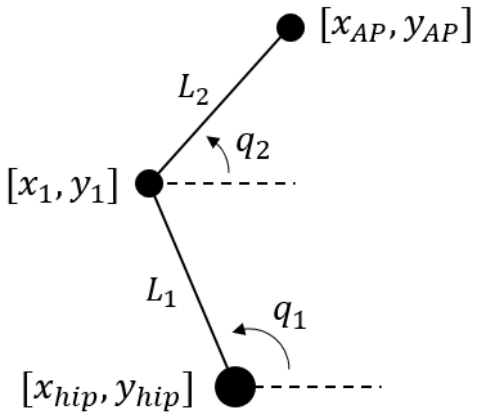

Figure B.3: Geometric model of the RRR exoskeleton in which AP is the attachment point where the exoskeleton and the human arm meet, L_1 is the length of the first exoskeleton link and L_2 is the length of the second exoskeleton link

B.1.2. RPR

For the RPR case the AP can be described in exoskeleton coordinates as well. This is done by the hand of figure B.4. The equations are defined as follows:

$$x_1 = x_{hip} + (L_1 + q_2) \cdot cos(q_1) \tag{B.7}$$
$$y_1 = y_{hip} + (L_1 + q_2) \cdot sin(q_1) \tag{B.8}$$

In which $[x_1, y_1]$ are the coordinates of the first joint, $[x_{hip}, y_{hip}]$ are the coordinates of the hip, L_1 is the length of the piston, L_2 is the length of the second exoskeleton link, q_1 is the angle of the piston w.r.t. the horizontal axis counter-clockwise positive and q_2 is the extension of the piston.

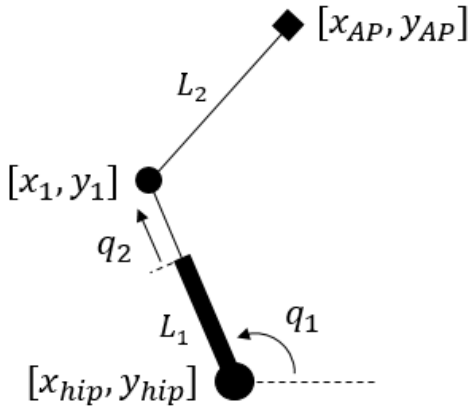

Figure B.4: Geometric model of the RPR exoskeleton in which AP is the attachment point where the exoskeleton and the human arm meet, L_1 is the length of the piston base and L_2 is the length of the second exoskeleton link

Note that in this particular case the angle of L_2 is the same as the angle of the human arm q_3 since the connection at the AP is fixed. This is indicated by the square in figure B.4. Two relations can be set up:

$$x_{AP} = x_{hip} + (L_1 + q_2) \cdot cos(q_1) + L_2 \cdot cos(q_3) \tag{B.9}$$
$$y_{AP} = y_{hip} + (L_1 + q_2) \cdot sin(q_1) + L_2 \cdot sin(q_3) \tag{B.10}$$
$$x_1 = x_{shoulder} + L_4 \cdot cos(q_3) + L_3 \cdot cos(q_3 - \frac{\pi}{2}) - L_2 \cdot cos(q_3) \tag{B.11}$$
$$y_1 = y_{shoulder} + L_4 \cdot sin(q_3) + L_3 \cdot sin(q_3 - \frac{\pi}{2}) - L_2 \cdot sin(q_3) \tag{B.12}$$

In which q_3, L_3 and L_4 are the angle of the arm, the distance from the AP to the human skeleton and the distance from the shoulder to L_3 as indicated in figure B.2. L_2 is the length of link two.

B.1.3. PRR

The AP of the PRR case in exoskeleton terms can be described by the hand of figure B.5 and the following equations:

$$x_1 = x_{hip} \tag{B.13}$$
$$y_1 = y_{hip} + q_1 \tag{B.14}$$
$$x_{AP} = x_1 + L_2 \cdot cos(q_2) \tag{B.15}$$
$$y_{AP} = y_1 + L_2 \cdot sin(q_2) \tag{B.16}$$

In which $[x_1, y_1]$ are the coordinates of the first joint, $[x_{hip}, y_{hip}]$ are the coordinates of the hip, L_1 is the length of the rail guiding the slider, L_2 is the length of the second exoskeleton link, q_1 is the position of

the slider with the hip location as origin and q_2 is the angle of L_2 measured from the horizontal axis where counter-clockwise is positive.

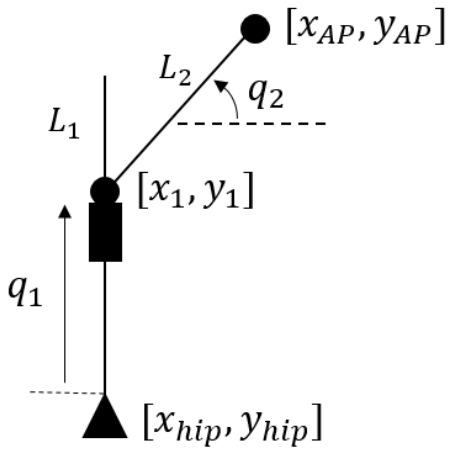

Figure B.5: Geometric model of the PRR exoskeleton in which AP is the attachment point where the exoskeleton and the human arm meet, L_1 is the length of the rail guiding the slider and L_2 is the length of the second exoskeleton link

B.2. Physical Boundaries

This section elaborates on how the physical boundaries that are used as a search space for the optimization problem are found. Each case is discussed separately. The design parameters are L_1, L_2 and AP. L_3 is fixed.

B.2.1. RRR

To define the physical boundaries for the RRR case the following was done: For multiple points p within the workspace $q_3 = [-85°, 85°]$ the AP is determined. These locations are defined by AP_p which is represented by $[x_{AP}, y_{AP}]_p$. This is done by equation B.1. In this work four points were evaluated. For each of these points the minimum distance to the circle defined by equation B.3 was determined, figure B.6 shows this in more detail.

The maximum of these minima will be the lower bound on L_2. This is due to the fact that if a smaller minima is chosen L_2 has to elongate to reach the positions that have a larger minimum distance to the circle. This is physically not possible. However to reach a position that has a lower minimum distance L_2 can move to a point on the circle defined by equation B.1 that is more distant to the location of the AP. This is further illustrated by figure B.7.

For the upper bound the same reasoning is used but now the other way around. For each of the locations AP_p the maximum distance to the circle is determined. The minimum of these maxima is used as an upper bound on L_2. And thus:

$$L_{2,min} = max(\, min(\, ||AP_p - a_{min,p}||_2)) \tag{B.17}$$

$$L_{2,max} = min(\, max(\, ||AP_p - a_{max,p}||_2)) \tag{B.18}$$

In which $L_{2,min}$ and $L_{2,max}$ are the lower and upper bound on L_2, AP_p is the attachment point evaluation at point p within the workspace and $a_{min,p}$ is the location on the circle for the minimum distance and $a_{max,p}$ is the point on the same circle for the maximum distance. This point is determined by equation B.3 with radius $L1, j$ at angle q_i.

For the physically possible values for L_1 the following holds: If for a particular $L_{1,j}$ the following holds: $L_{2,min} > L_{2,max}$ then $L_{1,j}$ is not physically possible.

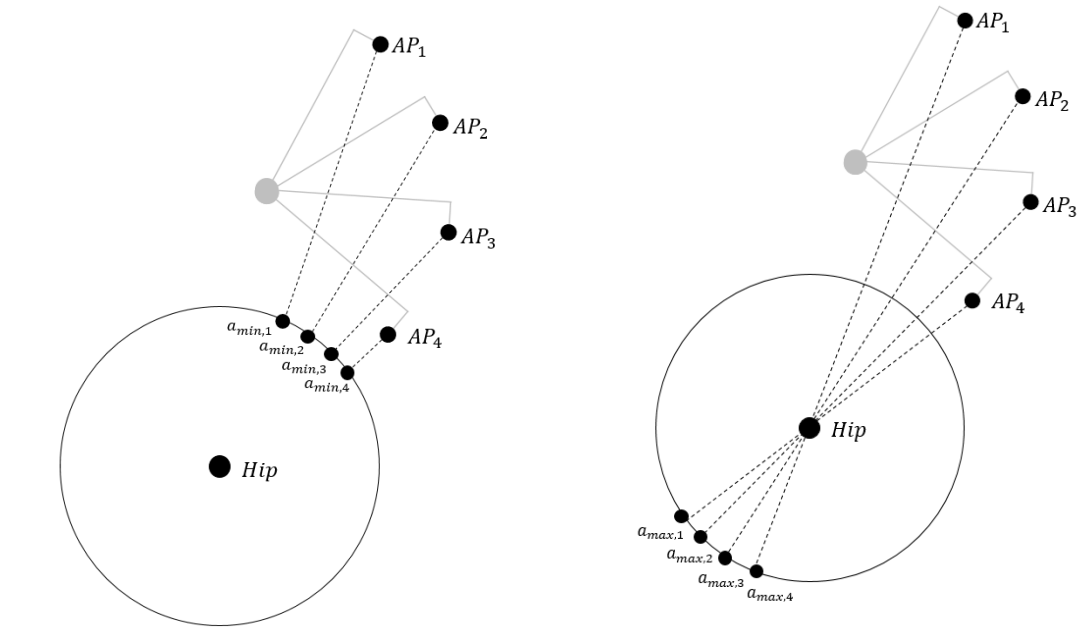

(a) (b)

Figure B.6: The minimum and maximum distance from four AP locations to the circle defined by B.3

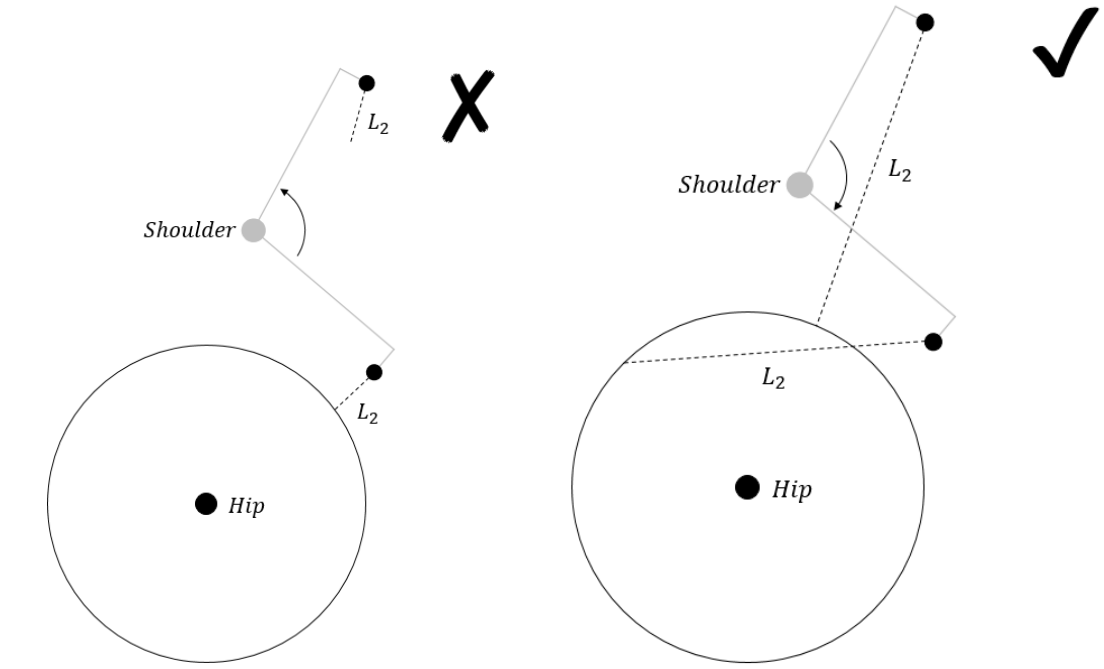

(a) (b)

Figure B.7: Graphical representation on physical limits on L_2 for the RRR case, in figure B.7a L_2 is too short when moving the arm, in figure B.7b this is possible

B.2.2. RPR

In the RPR case the exoskeleton and the human are attached at point $[x_1, y_1]$ (referred to as **b**) this is due to the fact that L_2 is fixed to the arm and does not change orientation w.r.t. the arm. The relation provided in equation B.9 is used that describes this point. Again this point is plotted for multiple locations in the workspace $q_3 = [-85°, 85°]$.

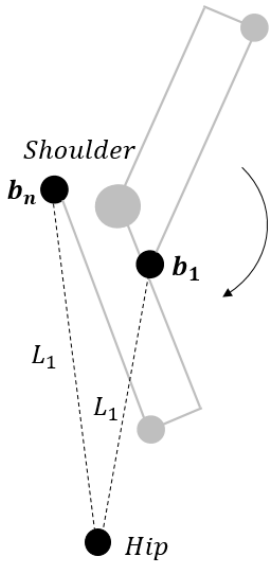

Figure B.8: Graphical representation of the location of point **b** throughout the workspace in which n indicates the $n-th$ point in this workspace

In this case four points are used. For this application a simple piston is assumed, meaning its maximum extension is equal to its length and it can not compress. In order to reach the entire workspace the following holds: The piston can not be longer than the minimum distance from the point **b**, described by equation B.9, to the hip. In other terms:

$$L_{1,max} = min(\,||\mathbf{b} - Hip||_2) \tag{B.19}$$

In which **b** is the point describing the point where the exoskeleton and the human arm are connected, Hip is the location of the hip and $L_{1,max}$ is the upper bound on L_1.

In order to determine the lower bound on L_1 and to determine the feasible set of L_2 use is made of the fact that the piston can only extend by its own lengths. This means that the maximum distance from point **b** to the hip has to be smaller or equal than twice the piston length:

$$max(\,||\mathbf{b} - Hip||_2)) \leq 2 \cdot L_1 \tag{B.20}$$

B.2.3. PRR

For the PRR case L_1 is the guiding rail for the slider. This rail is located at the hip and runs vertically. The maximum length of this link is the vertical distance from hip to shoulder since no material is desired above the shoulder. However if the slider has a maximum position lower than the shoulder this is used as the value for L_1 since the extra length is not used.

In order to determine the physically possible set of L_2 the following is done: A circle is drawn around the AP which is defined by B.1. This circle has radius L_2 and is evaluated at different values of L_2 ranging from $L_{2,j} = [L_{2,min}, L2, max]$, where $L_{2,j}$ is point j within the specified range. The intersection of this circle with the line described by $y = x_{hip}$ is determined. This intersection can either have two point, one point or no points. If one of the intersection points lies within the range $y = [y_{hip}, y_{shoulder}]$ for all AP within the workspace $q_3 = [-85°, 85°]$ then $L_{2,j}$ is a possible option. This is further illustrated by figure B.9 Hence the following relations must hold:

$$x_{AP} - L_{2,j} \cdot cos(q_2) = x_{hip} \tag{B.21}$$

$$y_{hip} \leq y_{AP} - L_{2,j} \cdot sin(q_2) \leq y_{shoulder} \tag{B.22}$$

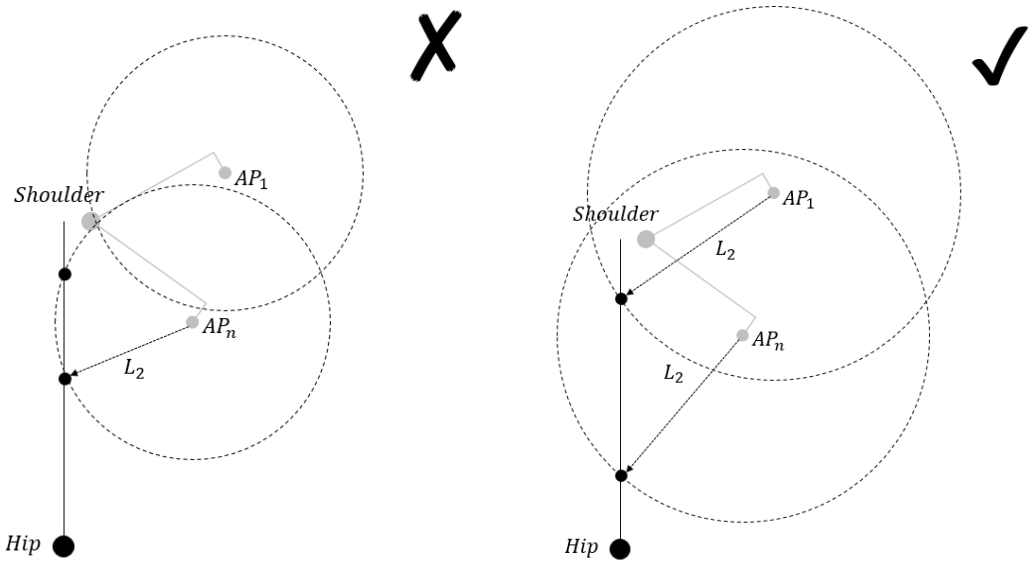

(a) (b)

Figure B.9: Graphical representation on physical limits on L_2 for the PRR case, in figure B.9a L_2 is too short when moving the arm, in figure B.9b this is possible

B.3. Results Link Length Analysis

This section shows the resulting physical link lengths calculated previously. First for the RRR case, followed by the RPR case and finally the PRR case. In all cases link three is taken as a constant and represents the thickness of the arm and the structure attached to the arm. These values are dependent on the chosen materials and the subjects arm width, for now a value of 0.1 $[m]$ is used to include for a large range of arm widths.

B.3.1. RRR

The lower and upper bounds of link two as a function of link one are shown in figure B.11. As can be seen the upper bound of link two is a linear function of link one and the attachment point. The lower boundary is a combination of two linear functions with a discontinuity. The function on the upper can be expressed as a function of link one and the minimum feasible length of link one, which in turn is a function of the attachment point (AP). The minimum link one length is described by:

$$L_{1,min} = 0.33 \cdot AP + 0.030 \tag{B.23}$$

This line is based on the regression line that describes the minimum feasible length of link one as a function of the attachment point as shown in figure B.10.

The maximum length of link one was not found for the investigated range of [0,2] The upper bound can then be described by

$$L_{2,ub} = 0.51 + (L_1 - L_{1,min}) \tag{B.24}$$

The lower bound has a discontinuity and can be described as:

$$L_{2,lb} = 0.51 - (L_1 - L_{1,min}) \qquad \forall L_1 \in [L_{1,min}, 0.51] \tag{B.25}$$

$$L_{2,lb} = 0.51 - (0.51 - L_{1,min}) + (L_1 - L_{1,min}) \qquad \forall L_1 \in [0.51, 2] \tag{B.26}$$

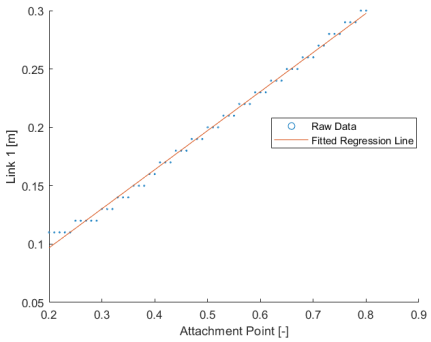

Figure B.10: Minimum feasible length of link one as a function of the attachment point

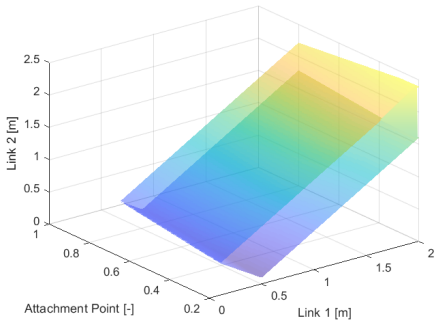

Figure B.11: lower and upper bounds on link two as a function of the attachment point and link one

B.3.2. RPR

For the RPR case there are a number of possible link two lengths that can be defined with an upper and lower bound on link one. Which is the other way around as before. The results of the RPR mechanism show a more non-linear result with discontinuities on the lower as well as the upper bound of link one. The boundaries of the feasible domain are shown in figure B.12.

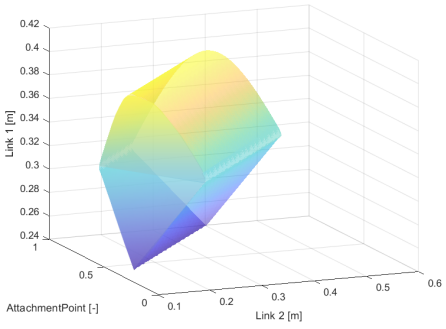

Figure B.12: lower and upper bounds on link one as a function of the attachment point and link two

The relation between the bounds of link one and the attachment point and link two are further investigated. A two dimensional plot is shown in figure B.13a to analyse the relation of link one and link two for different values of the attachment point. From figure B.13a it can be seen that the slope is the same for every attachment point and the peaks and valleys correspond as well. The minimum link two length determines the difference in starting points. The relation of the minimum link two length and the attachment point is shown in figure B.13b. This line can be modelled by:

$$L_{2,min} = 0.45 \cdot AP - 0.15 \tag{B.27}$$

The same can be done for the maximum value of link two, this line is equal to:

$$L_{2,max} = 0.45 \cdot AP + 0.14 \tag{B.28}$$

For all values of the attachment point below 0.59 the minimum value of link two is equal to 0.10 since this is the lowest investigated value. However for the calculation the virtual minimum of link two is used described by the line defined by B.27 since this makes the calculations less cumbersome. With this relation known the boundaries of link one can be described as follows:

$$L_{1,lb} = 0.32 - 0.50 \cdot (L_2 - L_{2,min}) \qquad \forall L_2 \in [L_{2,min}, L_{2,min} + \frac{R}{2}]$$

$$L_{1,lb} = 0.32 - 0.50 \cdot (\frac{R}{2} - L_{2,min}) + 0.50 \cdot (L_2 - L_{2,min}) \qquad \forall L_2 \in [L_{2,min} + \frac{R}{2}, L_{2,max}]$$

$$L_{1,ub} = 0.32 + 0.53 \cdot (L_2 - L_{2,min}) \qquad \forall L_2 \in [L_{2,min}, L_{2,min} + \frac{R}{2}]$$

$$L_{1,ub} = 0.32 + 0.53 \cdot (\frac{R}{2} - L_{2,min}) - 0.53 \cdot (L_2 - L_{2,min}) \qquad \forall L_2 \in [L_{2,min} + \frac{R}{2}, L_{2,max}]$$

Where R is the range between $L_{2,min}$ and $L_{2,max}$ which is equal to 0.29.

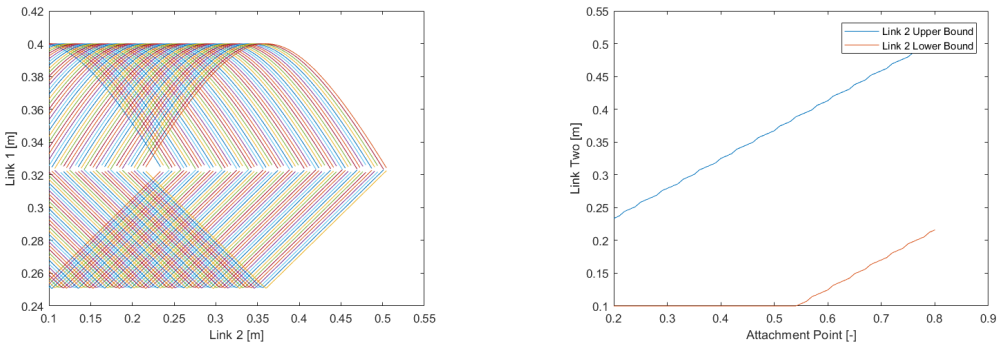

(a) (b)

Figure B.13: Two dimensional representation of the lower and upper bounds on link one as a function of the attachment point and link two in figure B.13a and the minimum length of link two as a function of the attachment point in figure B.13b

B.3.3. PRR

The PRR system is not bounded by a box but by a plane in space. The design options are significantly less then the options for the other two cases. The resulting plane can be seen in figure B.14.

link one is determined by taking the maximum point of the slider throughout the entire motion and has one unique value for every value of link two, hence the bound forms a plane. Note that the slider can be located at two different locations for each point throughout the motion except for the singular position. For the bounds the lowest of these two locations is used. link two does have an upper and a lower bound depending on the location of the attachment point. These bounds are shown in figure B.15a. These bounds can be approximated by two lines described by:

$$L_{2,min} = 0.29 \cdot AP + 0.16$$
$$L_{2,max} = -0.24 \cdot AP + 0.44$$

This relation holds only when $L_{2,max} \geq L_{2,min}$.

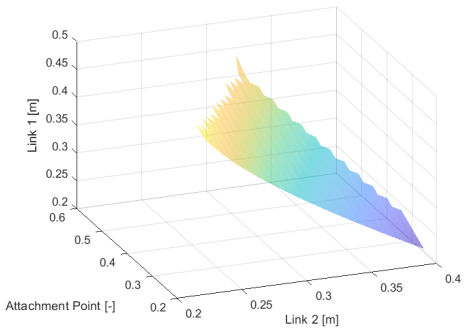

Figure B.14: bounds on link one, link two and the attachment point that have to be satisfied for a feasible PRR linkage

Figure B.15b shows the values of link one as a function of link two, this is plotted for different values of the attachment point. These lines can be approximated by a linear function. The link one value of the starting point is always equal to 0.50 and the slope of the lines is equal as well. The only value that changes is the $L_{2,min}$. Hence each line can be represented by the following equation:

$$L_1 = -0.12 + 0.51 - 1.16 \cdot (L_2 - L_{2,min}) \quad \forall L_{2,min} \leq L_{2,max} \tag{B.29}$$

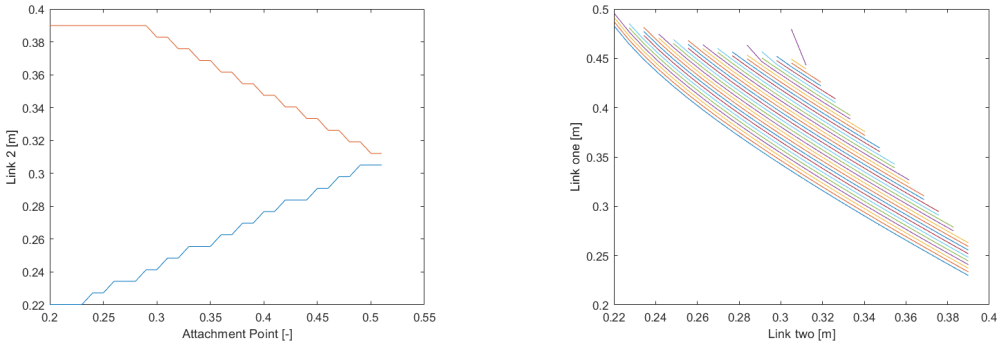

(a) (b)

Figure B.15: Two dimensional representation of the bounds on link two as a function of the attachment point for the PRR case in figure B.15a and Link one as a function of link two plotted for different values of the attachment point in figure B.15b

C

Application to Shoulder Exoskeleton: Optimization

This section elaborates on the optimization process. First the derivation of the objective functions are shown. The constraints that are used a presented and the optimization is formulated in the formal way.

C.1. Objective Function

A multi objective optimization is performed in chapter 3. Four objectives are presented with their mathematical expression. This section elaborates on the derivation of the objective functions. In the formal representation of a multi objective optimization problem the objective function is written as:

$$\mathbf{f}(\mathbf{x}) = f_1(\mathbf{x}) + f_2(\mathbf{x}) + ... + f_n(\mathbf{x}) \tag{C.1}$$

in which n is the number of objectives. In this optimization problem four objectives are minimized these objectives are discussed in the following sections.

C.1.1. Total Link Length

The first objective function is the total length of the optimized parameters L_1, L_2 and AP. This can be written as an objective function as follows:

$$f_1(\mathbf{x}) = L_1 + L_2 + AP \cdot L_{arm} \tag{C.2}$$

In which L_{arm} is the length of the arm.

C.1.2. Workspace Area

The workspace of the entire system (i.e. the closed system of the human arm and the exoskeleton) is used as a measure of fitness in the optimization. In order to make a representation of the workspace area the human arm and the exoskeleton are divided into two separate systems. This is done by making a cut at the connection point in the arm.

For the RRR case this means that the end effector of the exoskeleton is described by the AP in equation B.3 and the end effector of the arm is the AP described by equation B.1.

For the RPR case the end effector location of the exoskeleton corresponds to the location of joint one and can be described by equation B.7. The end effector of the arm can be described by equation B.9.

For the PRR case the end effector location of the exoskeleton is the same as the attachment point and can be described by equation B.13. The end effector of the arm is the same as in the RRR case and is described by equation B.1.

For every iteration the full range of motion of the human joint is simulated. In the case of the shoulder it is assumed that this is from $q_3 = [-85°, 85°]$. In which 0° is with the arm horizontal. The misalignment joints are simulated by moving the origin of the shoulder over a specified range of translations. This range is specified by: [0.5 $[m]$, 0.55 $[m]$] in x-direction [2, 23] and [0.09 $[m]$, 0.11 $[m]$] in y-direction [2, 11]. Evaluating B.1 and B.7 for all values within these ranges this results in a workspace area of the arm: w_{arm}.

Next to the arm also the full r.o.m. of the exoskeleton is simulated. For the revolute joints this is a whole circle and for the prismatic joints this is a range that is defined by the physical limits of the structure. Equation B.3, B.9 and B.13 are evaluated over the entire range of q_1 and q_2, which is equal to $q = [0, 2\pi]$ for revolute joints and $q = [0, L]$ for prismatic joints, in which L is the maximum position of the slider. This results in an area in space which is the exoskeleton workspace are which is defined as: w_{exo}.

The workspace area $A_{workspace}$ can then be defined as the overlap between the exoskeleton workspace area and the workspace area of the arm:

$$A_{workspace} = w_{arm} \cap w_{exo} \tag{C.3}$$

This workspace however scales differently with different locations of the attachment point and hence the workspace is taken as a percentage of the arm workspace to give a proper indication of how much of the desired arm movements can be achieved.

$$W_{workspace} = \frac{A_{workspace}}{w_{arm}} \tag{C.4}$$

Furthermore the algorithm used is one that minimizes the objective function and hence the inverse relation of this workspace percentage can be minimized. The objective function becomes:

$$f_2(\mathbf{x}) = \frac{w_{arm}}{A_{workspace}} \tag{C.5}$$

C.1.3. Distance to the Body

The second objective is the distance to the body of the exoskeleton. This distance can be represented by the whole structure. However the location of the structure, at least when assuming straight elements, is directly related to the location of the joints. Hence this is used as an objective. The distance of the structure is dependent on the location of the middle joint in all three cases. The body is represented by a straight line going through the arm and the hip.

In the RRR case the location of the middle joint can be described by equation B.3. In the RPR case equation B.7 is used and for the PRR case equation B.13 is used. With these equations the joint locations can be determined for the union of the workspaces calculated before. Since these are the only locations of interest. The distance to the body can now be easily expressed by taking the projection of each vector from the hip to each joint location i.

$$proj_i = \mathbf{a}_i \cdot \frac{\mathbf{b}}{||\mathbf{b}||} \tag{C.6}$$

in which $\mathbf{a}_i$ is the vector from the hip to joint location i. $\mathbf{b}$ is the vector from the hip to the arm and $proj_i$ is the magnitude of the projection of the vector from the hip to joint i on the vector from the hip the the arm. Then:

$$\mathbf{proj}_i = proj_i \cdot \frac{\mathbf{b}}{||\mathbf{b}||} \tag{C.7}$$

and the vector that represents the distance to the line from joint i is determined by:

$$\mathbf{distance}_i = \mathbf{a}_i - \mathbf{proj}_i \tag{C.8}$$

the magnitude of the distance is then simply the norm of $\mathbf{distance}_i$. The objective function is then simply described by:

$$f_3(\mathbf{x}) = \frac{1}{n}\sum_{i}^{n} ||\mathbf{distance}_i||_2 \tag{C.9}$$

where n is the total number of joint locations.

C.1.4. Singularities

To detect singularities the jacobian can be used. If the jacobian can not be inverted a singular position has been reached. This happens when the determinant of the jacobian is equal to zero. The jacobian of each configuration is determined. For the RRR case the jacobian becomes:

$$J_{RRR} = \begin{bmatrix} -l_1 \cdot sin(q_1) & -l_2 \cdot sin(q_2) \\ l_1 \cdot cos(q_1) & l_2 \cdot cos(q_2) \end{bmatrix}$$

The RPR case is a little different since the cut is made before link two. For the singularity analysis link two has to be taken into account and the angle of link two is the same as that of the arm angle q_3. Singularities are only dependent on the angle of the first link and the angle of the second link not on the piston. hence the term $(l_1 + q_2)$ is replaced by c_1 for simplicity. The jacobian then becomes.

$$J_{RPR} = \begin{bmatrix} -c_1 \cdot sin(q_1) & -l_2 \cdot sin(q_3) \\ c_1 \cdot cos(q_1) & l_2 \cdot cos(q_3) \end{bmatrix}$$

And the PRR case is equal to:

$$J_{PRR} = \begin{bmatrix} 0 & -l_2 \cdot sin(q_2) \\ 1 & l_2 \cdot cost(q_2) \end{bmatrix}$$

Then for the singular positions the following holds:

$$det(J_n) = 0 \tag{C.10}$$

in which n denotes the configuration (n= RRR, RPR or PRR). This position has to be avoided and this can be translated into an objective function as:

$$obj_{singularities} = \frac{1}{|det(J_i)|} \tag{C.11}$$

This objective however scales differently for changing ratios of link one and link two. Hence a dimensionless objective can be made for each different case:

$$f_{4,RRR}(\mathbf{x}) = \frac{L_1 \cdot L_2}{|det(J_i)|} \tag{C.12}$$

$$f_{4,RPR}(\mathbf{x}) = \frac{c_1 \cdot L_2}{|det(J_i)|} \tag{C.13}$$

$$f_{4,PRR}(\mathbf{x}) = \frac{L_2}{|det(J_i)|} \tag{C.14}$$

C.2. Constraints

The constraints on the optimizations are defined by the upper and lower bounds on the link lengths. Since this are (non-linear) functions they can not be included by simple bounds but have to be implemented as constraints. These constraints are equal to the boundaries defined by the physically feasible set shown in B. There are inequality and equality constraints and the difference between linear and non linear constraints can be made. Linear equality constraints can be written in the form:

$$A\mathbf{x} = \mathbf{b} \tag{C.15}$$

In which $\mathbf{x}$ is the parameter vector, which is equal to: $\mathbf{x} = [L_1, L_2, AP]$. The linear inequality constraints are written in the form:

$$A\mathbf{x} \leq \mathbf{b} \tag{C.16}$$

The non linear equality constraints are written in the form:

$$g(\mathbf{x}) = 0 \tag{C.17}$$

And finally the non linear inequality constraints are in the form:

$$g(\mathbf{x}) \leq 0 \tag{C.18}$$

With these constraints and the objective functions the formal representation of the optimization problem for the RRR case is as follows:

$$\begin{aligned} \min_{\mathbf{x}} \quad & f_1(\mathbf{x}) + f_2(\mathbf{x}) + f_{3,RRR}(\mathbf{x}) + f_4(\mathbf{x}) \\ \text{subject to} \quad & A_{RRR}\mathbf{x} \leq b_{RRR} \\ & g_1(\mathbf{x})_{RRR} \leq 0 \\ & g_2(\mathbf{x})_{RRR} \leq 0 \end{aligned}$$

For the RPR case the problem becomes:

$$\begin{aligned} \min_{\mathbf{x}} \quad & f_1(\mathbf{x}) + f_2(\mathbf{x}) + f_{3,RPR}(\mathbf{x}) + f_4(\mathbf{x}) \\ \text{subject to} \quad & A_{RPR}\mathbf{x} \leq b_{RPR} \\ & g_1(\mathbf{x})_{RPR} \leq 0 \\ & g_2(\mathbf{x})_{RPR} \leq 0 \\ & g_3(\mathbf{x})_{RPR} \leq 0 \\ & g_4(\mathbf{x})_{RPR} \leq 0 \end{aligned}$$

And for the PRR case this becomes:

$$\begin{aligned} \min_{\mathbf{x}} \quad & f_1(\mathbf{x}) + f_2(\mathbf{x}) + f_{3,PRR}(\mathbf{x}) + f_4(\mathbf{x}) \\ \text{subject to} \quad & A_{PRR}\mathbf{x} \leq b_{PRR} \\ & A_{eq,PRR}\mathbf{x} \leq b_{eq,PRR} \end{aligned}$$

The definitions of these constraints are presented in the following section.

C.2.1. RRR

For the linear inequality constraints of the RRR case:

$$A_{RRR} = \begin{bmatrix} -1 & 0 & 0.44 \\ -1 & 1 & 0.44 \end{bmatrix} \tag{C.19}$$

$$b_{RRR} = \begin{bmatrix} -0.025 \\ 0.51 - 0.025 \end{bmatrix} \tag{C.20}$$

The non linear inequality constraints become:

$$g_1(\mathbf{x})_{RRR} = 0.50 - (L_1 - L_{1,min}) - L_2 \qquad \forall L_1 \in [L_{1,min}, 0.51] \tag{C.21}$$

$$g_2(\mathbf{x})_{RRR} = 0.50 - (0.51 - L_{1,min}) + (L_1 - L_{1,min}) - L_2 \qquad \forall L_1 \in [0.51, 2] \tag{C.22}$$

C.2.2. RPR

The same set of equations is determined for the RPR case, for the linear inequality constraints matrix A becomes:

$$A_{RPR} = \begin{bmatrix} 0 & -1 & 0.45 \\ 0 & 1 & -0.45 \end{bmatrix} \tag{C.23}$$

$$b_{RPR} = \begin{bmatrix} 0.15 \\ 0.14 \end{bmatrix} \tag{C.24}$$

The non linear inequality constraints are:

$$g_1(\mathbf{x})_{RPR} = 0.32 - 0.50 \cdot (L_2 - L_{2,min}) - L_1 \qquad \forall L_2 \in [L_{2,min}, L_{2,min} + \frac{R}{2}] \tag{C.25}$$

$$g_2(\mathbf{x})_{RPR} = 0.32 - 0.50 \cdot (\frac{R}{2} - L_{2,min}) + 0.50 \cdot (L_2 - L_{2,min}) - L_1 \qquad \forall L_2 \in [L_{2,min} + \frac{R}{2}, L_{2,max}] \tag{C.26}$$

$$g_3(\mathbf{x})_{RPR} = -0.32 - 0.53 \cdot (L_2 - L_{2,min}) + L_1 \qquad \forall L_2 \in [L_{2,min}, L_{2,min} + \frac{R}{2}] \tag{C.27}$$

$$g_4(\mathbf{x})_{RPR} = -0.32 - 0.53 \cdot (\frac{R}{2} - L_{2,min}) + 0.53 \cdot (L_2 - L_{2,min}) + L_1 \qquad \forall L_2 \in [L_{2,min} + \frac{R}{2}, L_{2,max}] \tag{C.28}$$

Where R is the range between $L_{2,min}$ and $L_{2,max}$ which is equal to 0.29.

C.2.3. PRR

Finally for the PRR case the linear inequality constraints are equal to:

$$A_{PRR} = \begin{bmatrix} 0 & 1 & 0.32 \\ 0 & -1 & 0.39 \end{bmatrix} \tag{C.29}$$

$$b_{PRR} = \begin{bmatrix} 0.43 \\ -0.057 \end{bmatrix} \tag{C.30}$$

the PRR case doest not have any non linear constraints, however there is one set of linear equality constraints:

$$A_{eq,PRR} = \begin{bmatrix} 1 & 1.2 & -0.45 \end{bmatrix} \tag{C.31}$$

$$b_{eq,PRR} = \begin{bmatrix} 0.57 \end{bmatrix} \tag{C.32}$$

D

Application to Shoulder Exoskeleton: Verification

For the verification of the results of the synthesis two configurations are tested. One for the RRR case and one for the PRR case. The choice of configuration is mainly based on the ease of generating a linear moment profile for the joints. This was done by analysing the stiffness in the joints required for balancing. Which is part of the force analysis and discussed in further detail later in this thesis.

The reason for wanting a linear profile is that this is the simplest way to verify that the force analysis is correct. To complete both the verification of the optimization results and the force analysis results without the need of making new parts this moment profile is already taken into account.

Furthermore A sensitivity analysis was performed on the results. Since the optimization space is unknown and likely to be very non-linear a sensitivity analysis is done of small uncertainties which could arise during production, errors due to approximations made and numerical errors. Uncertainties of up to 1 [%] are investigated. This uncertainty is evaluated each optimization parameter separately. First an uncertainty is added to link one, then to link two and finally the attachment point.

The evaluation is done by adding $[-1,1]$ [%] to the corresponding parameter and evaluating the objective function with the new parameters that include this objective $\tilde{\mathbf{x}}_j$. For each objective the sensitivity is expressed in its maximum deviation from the original solution $\mathbf{x}^*$. This deviation is expressed as a percentage of the original fitness value $f_i(\mathbf{x}^*)$ where i is the objective number, so:

$$S_{ij} = \frac{f_i(\mathbf{x}^*) - f_i(\tilde{\mathbf{x}}_j)}{f_i(\mathbf{x}^*)} \cdot 100\% \tag{D.1}$$

Bibliography

[1] Cover Image. URL https://www.timetoast.com/timelines/human-vs-machine.

[2] Dined. URL https://dined.io.tudelft.nl/en/database/introduction.

[3] No Title. URL https://www.cbs.nl/nl-nl/nieuws/2012/49/nederlanders-steeds-langer-maar-vooral-zwaarder

[4] Stephen Bevan. The Impact of Back Pain on Sickness Absence in Europe. *The Work Foundation ,Reports*, 1(June):3–8, 2012.

[5] Marco Cempini, Stefano Marco Maria De Rossi, Tommaso Lenzi, Nicola Vitiello, and Maria Chiara Carrozza. Self-alignment mechanisms for assistive wearable robots: A kinetostatic compatibility method. *IEEE Transactions on Robotics*, 29(1):236–250, 2013. ISSN 15523098. doi: 10.1109/TRO.2012.2226381.

[6] Marco Cempini, Mario Cortese, and Nicola Vitiello. A powered finger-thumb wearable hand exoskeleton with self-aligning joint axes. *IEEE/ASME Transactions on Mechatronics*, 20(2):705–716, 2015. ISSN 10834435. doi: 10.1109/TMECH.2014.2315528.

[7] Zhuoqi Cheng, Shaohui Foong, Defeng Sun, and U. Xuan Tan. Towards a multi-DOF passive balancing mechanism for upper limbs. *IEEE International Conference on Rehabilitation Robotics*, 2015-Septe: 508–513, 2015. ISSN 19457901. doi: 10.1109/ICORR.2015.7281250.

[8] Charles E Clauser, John T McConville, and J W Young. Weight, Volume, and Center of Mass of Segments of the Human Body. *National Technical Information Service*, pages 1–112, 1969. ISSN 1076-2752. doi: AMRL-TR-69-70(AD710622).

[9] Nick Van Dijk. Wearable Passive Upper Extremity Exoskeletons for the Shoulder : A Review. pages 1–7.

[10] A G Dunning. *Slender spring systems*. 2016. ISBN 9789461866110.

[11] H. Graichen, S. Hinterwimmer, R. Von Eisenhart-Rothe, T. Vogl, K. H. Englmeier, F. Eckstein, D.T. Harryman, J.a. Sidles, J.M. Clark, K.J. McQuade, T.D. Gibb, and F.a Matsen. Translation of the humeral head with passive glenohumeral on the glenoid motion. *Journal of Biomechanics*, 38(4):1334–1343, 2005. ISSN 00219290. doi: 10.1016/j.jbiomech.2004.05.020.

[12] E. Grandjean and W. Hünting. Ergonomics of posture-Review of various problems of standing and sitting posture. *Applied Ergonomics*, 8(3):135–140, 1977. ISSN 00036870. doi: 10.1016/0003-6870(77)90002-3.

[13] Erico Guizzo and Harry Goldstein. The rise of the body bots. *IEEE Spectrum*, 42(10):50–56, 2005. ISSN 00189235. doi: 10.1109/MSPEC.2005.1515961.

[14] J A Hidalgo, A M Genaidy, R Huston, and J Arantes. Occupational biomechanics of the neck: a review and recommendations, 1992. ISSN 03008134.

[15] Larry L Howell. Introduction to Compliant Mechanisms Mechanisms. 2013.

[16] Hsiang-Chien Hsieh and Chao-Chieh Lan. A lightweight gravity-balanced exoskeleton for home rehabilitation of upper limbs. *2014 IEEE International Conference on Automation Science and Engineering (CASE)*, pages 972–977, 2014. doi: 10.1109/CoASE.2014.6899444. URL http://ieeexplore.ieee.org/lpdocs/epic03/wrapper.htm?arnumber=6899444.

[17] Hsiang Chien Hsieh, Dian Fu Chen, Li Chien, and Chao Chieh Lan. Design of a Parallel Actuated Exoskeleton for Adaptive and Safe Robotic Shoulder Rehabilitation. *IEEE/ASME Transactions on Mechatronics*, 22(5):2034–2045, 2017. ISSN 10834435. doi: 10.1109/TMECH.2017.2717874.

[18] Ulf Järvholm, Jorma Styf, Madis Suurkula, and Peter Herberts. Intramuscular pressure and muscle blood flow in supraspinatus. *European Journal of Applied Physiology and Occupational Physiology*, 58(3): 219–224, 1988. ISSN 03015548. doi: 10.1007/BF00417252.

[19] W. Karwowski. Ergonomics and human factors: The paradigms for science, engineering, design, technology and management of human-compatible systems. *Ergonomics*, 48(5):436–463, 2005. ISSN 00140139. doi: 10.1080/00140130400029167.

[20] Yuichi Kurita, Jumpei Sato, Takayuki Tanaka, Minoru Shinohara, and Toshio Tsuji. Unpowered Sensorimotor-Enhancing Suit Reduces Muscle Activation and Improves Force Perception. *IEEE Transactions on Human-Machine Systems*, pages 1–6, 2017. ISSN 21682291. doi: 10.1109/THMS.2017.2700437.

[21] Britt Larsson, Karen Søgaard, and Lars Rosendal. Work related neck-shoulder pain: a review on magnitude, risk factors, biochemical characteristics, clinical picture and preventive interventions. *Best Practice and Research: Clinical Rheumatology*, 21(3):447–463, 2007. ISSN 15216942. doi: 10.1016/j.berh.2007.02.015.

[22] Michiel P De Looze, Frank Krause, and Leonard W O Sullivan. Wearable Robotics: Challenges and Trends. 16:195–199, 2017. doi: 10.1007/978-3-319-46532-6. URL `http://link.springer.com/10.1007/978-3-319-46532-6`.

[23] Amy Cole Lukasiewicz, Philip McClure, Lori Michener, Neal Pratt, Brian Sennett, Paula Ludewig, Amy Cole Lukasiewicz, Philip McClure, Lori Michener, Neal Pratt, and Brian Sennett. Comparison of 3-Dimensional Scapular Position and Orientation Between Subjects With and Without Shoulder Impingement. *Journal of Orthopaedic & Sports Physical Therapy*, 29(10):574–586, 1999. ISSN 0190-6011. doi: 10.2519/jospt.1999.29.10.574. URL `http://www.jospt.org/doi/10.2519/jospt.1999.29.10.574`.

[24] R. T. Marler and J. S. Arora. Survey of multi-objective optimization methods for engineering. *Structural and Multidisciplinary Optimization*, 26(6):369–395, 2004. ISSN 1615147X. doi: 10.1007/s00158-003-0368-6.

[25] National Research Council & Institute of Medicine. *MUSCULOSKELETAL DISORDERS AND THE WORKPLACE: Low Back and Upper Extremities*. 2001. ISBN 030951178X.

[26] Agnès Parent-Thirion, Greet Vermeylen, Gijs van Houten, Maija Lyly-Yrjänäinen, Isabella Biletta, Jorge Cabrita, and Isabelle Niedhammer. *Fifth european working conditions survey*. 2012. ISBN 9789289710626.

[27] L. Punnett, L. J. Fine, W. Monroe Keyserling, G. D. Herrin, and D. B. Chaffin. Shoulder disorders and postural stress in automobile assembly work. *Scandinavian Journal of Work, Environment and Health*, 26(4):283–291, 2000. ISSN 03553140. doi: 10.5271/sjweh.544.

[28] Laura Punnett and David H. Wegman. Work-related musculoskeletal disorders: The epidemiologic evidence and the debate. *Journal of Electromyography and Kinesiology*, 14(1):13–23, 2004. ISSN 10506411. doi: 10.1016/j.jelekin.2003.09.015.

[29] V Putz-Anderson, Bp Bernard, and Se Burt. Musculoskeletal disorders and workplace factors. ... *-Related Musculoskeletal ...*, 97-141(July 1997):1–1 – 7–11, 1997. URL `http://scholar.google.com/scholar?hl=en{&}btnG=Search{&}q=intitle:Musculoskeletal+disorders+and+workplace+factors{#}1{%}5Cnhttp://www.cdc.gov/niosh/docs/97-141/pdfs/97-141.pdf`.

[30] V Putz-Anderson, Bp Bernard, and Se Burt. Musculoskeletal disorders and workplace factors. ... *-Related Musculoskeletal ...*, 97-141(July 1997):1–1 – 7–11, 1997. URL `http://scholar.google.com/scholar?hl=en{&}btnG=Search{&}q=intitle:Musculoskeletal+disorders+and+workplace+factors{#}1{%}5Cnhttp://www.cdc.gov/niosh/docs/97-141/pdfs/97-141.pdf`.

[31] L. Schwab and Martin Wisse. Lecture Notes: Multibody Dynamics B. 1998.

[32] Barbara Silverstein and Darrin Adams. Work-related Musculoskeletal Disorders of the Neck , Back , and Upper Extremity in Washington State ,. (40):1997–2005, 2007.

[33] Arno H.A. Stienen, Edsko E.G. Hekman, Frans C.T. Van Der Helm, and Herman Van Der Kooij. Short Papers of Joint Rotations and Translations. 25(3):628–633, 2009.

[34] Sheryl S. Ulin, Thomas J. Armstrong, Stover H. Snook, and W. Monroe Keyserling. Perceived exertion and discomfort associated with driving screws at various work locations and at different work frequencies. *Ergonomics*, 36(7):833–846, 1993. ISSN 13665847. doi: 10.1080/00140139308967946.

[35] Henk F van der Molen, Chiara Foresti, Joost G Daams, Monique H W Frings-Dresen, and P Paul F M Kuijer. Work-related risk factors for specific shoulder disorders: a systematic review and meta-analysis. *Occupational and Environmental Medicine*, (i):oemed–2017–104339, 2017. ISSN 1351-0711. doi: 10.1136/oemed-2017-104339. URL http://oem.bmj.com/lookup/doi/10.1136/oemed-2017-104339.

[36] D Van Eerd, C Munhall, E Irvin, D Rempel, S Brewer, A J van der Beek, J T Dennerlein, J Tullar, K Skivington, C Pinion, and B Amick. Effectiveness of workplace interventions in the prevention of upper extremity musculoskeletal disorders and symptoms: an update of the evidence. *Occupational and Environmental Medicine*, 73(1):62–70, 2016. ISSN 1351-0711. doi: 10.1136/oemed-2015-102992. URL http://oem.bmj.com/lookup/doi/10.1136/oemed-2015-102992.

[37] Rogier M. Van Rijn, Bionka Ma Huisstede, Bart W. Koes, and Alex Burdorf. Associations between work-related factors and specific disorders of the shoulder - A systematic review of the literature. *Scandinavian Journal of Work, Environment and Health*, 36(3):189–201, 2010. ISSN 03553140. doi: 10.1093/rheumatology/kep013.

[38] Di Wang, Fei Dai, and Xiaopeng Ning. Risk Assessment of Work-Related Musculoskeletal Disorders in Construction: State-of-the-Art Review. *Journal of Construction Engineering and Management*, 141 (6):04015008, 2015. ISSN 0733-9364. doi: 10.1061/(ASCE)CO.1943-7862.0000979. URL http://ascelibrary.org/doi/10.1061/{%}28ASCE{%}29CO.1943-7862.0000979.

[39] Steven F. Wiker, Don B. Chaffin, and Gary D. Langolf. Shoulder posture and localized muscle fatigue and discomfort. *Ergonomics*, 32(2):211–237, 1989. ISSN 13665847. doi: 10.1080/00140138908966080.

[40] David A Winter. *Biomechanics and Motor Control of Human Movement*. 2005. ISBN 0-471-44989-X.

[41] Yue-Qing Yu, Larry L. Howell, Craig Lusk, Ying Yue, and Mao-Gen He. Dynamic Modeling of Compliant Mechanisms Based on the Pseudo-Rigid-Body Model. *Journal of Mechanical Design*, 127(4):760, 2005. ISSN 10500472. doi: 10.1115/1.1900750. URL http://mechanicaldesign.asmedigitalcollection.asme.org/article.aspx?articleid=1448594.

[42] M. Zhang, A. R. Turner-Smith, and V. C. Roberts. The Reaction of Skin and Soft Tissue to Shear Forces Applied Externally to the Skin Surface. *Proceedings of the Institution of Mechanical Engineers, Part H: Journal of Engineering in Medicine*, 208(4):217–222, 1994. ISSN 20416518. doi: 10.1243/PIME_PROC_1994_208_291_02.